Sedimentary Geology 334 (2016) 34–52

Contents lists available at ScienceDirect

Sedimentary Geology

journal homepage: www.elsevier.com/locate/sedgeo

Halokinetic sequences in carbonate systems: An example from the Middle Albian Bakio Breccias Formation (Basque Country, Spain)

Poprawski Yohann [a], Basile Christophe [b], Jaillard Etienne [b], Gaudin Matthieu [c], Lopez Michel [d]

[a] Institute of Earth Sciences Jaume Almera, ICTJA-CSIC, Group of Dynamics of the Lithosphere, Spain
[b] Joseph Fourier University, ISTerre, France
[c] Tullow Oil, Norge AS, Norway
[d] Montpellier 2 University, Géosciences Montpellier, France

ARTICLE INFO

Article history:
Received 5 November 2015
Received in revised form 15 January 2016
Accepted 17 January 2016
Available online 22 January 2016

Editor: B. Jones

Keywords:
halokinetic sequence
redeposited carbonates
diapir growth
carbonate platform
gravity-driven deposits
growth strata

ABSTRACT

In diapir flanks, unconformity-bounded sedimentary packages associated with gravity-driven deposits, controlled by the ratio between the rates of sediment accumulation and diapir growth can be interpreted in the context of halokinetic sequences. The Bakio Breccias Formation (Basque Country, Spain) corresponds to redeposited carbonate deposit that developed in response to the Bakio diapir growth during the Middle Albian. These deposits provide on of the rare documented example of carbonate-dominated halokinetic sequences. The Bakio Breccias Formation consists of an alternation of clast- and matrix-supported breccias, calcirudite, calcarenite and marl, deposited along the flanks of the diapir. The description and the analysis of the Bakio Breccias Formation lead to a new model for carbonate-dominated halokinetic sequences. These sequences differ from their siliciclastic counterpart because sediment accumulation rate is controlled by carbonate platform growth on the topographic relief top of the diapirs, while sediments are preferentially deposited in the mini-basins adjacent of the diapirs, in siliciclastic settings. During transgressive system tract, carbonate platform are able to keep up with the sea level rise and to aggrade on top of the diapirs, forming thick and resistant roof, which is assumed to limit the diapir growth and thus to favour the development of halokinetic sequences with low angle unconformities (wedge halokinetic sequences). During late highstand system tract deposition (and lowstand system tract if present), platform progradation results in high sediment accumulation in the adjacent depocenters, loading the autochthonous salt layer and promote diapir growth and creation of topographic relief. In addition, if the diapir roof reaches emersion, karstification of the carbonate platform top may also favour roof destruction and diapir growth. Depending on the thickness of the roof developed previously and the amplitude of the sea level fall, the halokinetic sequences with the emersion and the karstification of the carbonate platform may display high angle unconformities (hook halokinetic sequences). Furthermore, gravity-driven deposits are assumed to be more common in carbonate-dominated halokinetic sequences, compared to their siliciclastic counterparts, since carbonate platform aggradation creates steep slopes on the diapir margins, leading to the partial collapse of the margin, even when limited diapir growth occurs. The carbonate-dominated halokinetic sequence model proposed here is an important tool for the prediction of potential reservoir distribution, seal and hydrocarbon migration in flanks of salt diapirs where carbonate platform developed.

1. Introduction

Halokinetic sequences are unconformity-bounded sedimentary packages related to sediment destabilizations during drape folding associated with the diapir flank rotation. The model of halokinetic sequences (Giles and Lawton, 2002; Rowan et al., 2003) is based on the ratio between relative sediment accumulation rate and diapir rise rate. When diapir rise exceeds sediment accumulation, the diapir produces positive topographic relief and upturned flanking strata. Uplift of the diapir roof may induce instability leading to gravity flows or slumps. When sediment accumulation rate overcome the diapir rise rate, the diapir may be buried and the sediment accumulating on the diapir flanks remains relatively more stable. Since the pioneer works of Giles and Lawton (2002); Schultz-Ela (2003); Rowan et al. (2003); Giles and Rowan (2012), who proposed the drape fold and the halokinetic sequence models in the La Popa basin in Mexico, recent outcrop studies demonstrated the usefulness of this model in the same basin (Andrie et al., 2012; Rowan et al., 2012a), in the Basque-Cantabrian basin in Spain (Arbués et al., 2012; Rowan et al., 2012b; Poprawski et al., 2014; Ferrer et al., 2014), in the Central High Atlas in Morocco (Saura et al., 2014; Vergés et al., 2013), in the Sivas basin in Turkey (Callot et al., 2014; Ribes et al., 2015) and in Australia (Kernen et al., 2012; Hearon et al., 2014a, 2015). However published studies describe shallow-water siliciclastic or mixed systems (Giles and Lawton,

http://dx.doi.org/10.1016/j.sedgeo.2016.01.013
0037-0738/

2002; Rowan et al., 2003; Andrie et al., 2012; Giles and Rowan, 2012; Kernen et al., 2012; Rowan et al., 2012a; Callot et al., 2014), and deep-water environments (Arbués et al., 2012; Rowan et al., 2012b; Hearon et al., 2014b; Poprawski et al., 2014; Ferrer et al., 2014), but few outcrop-based examples in pure carbonate settings have been recognized. The halokinetic sequence models (Giles and Lawton, 2002; Rowan et al., 2003; Giles and Rowan, 2012) refer to siliciclastic sediments, where an external sedimentary source fills the mini-basins. In carbonate systems, sedimentation rates are higher in the topographic highs, where carbonate platform are able to develop. This is the case for several diapirs worldwide, where synkinematic isolated carbonate platform developed (e.g. Davison et al., 1996; Fernández-Mendiola and García-Mondéjar, 1997; Bantan, 1999; Bosence et al., 1998; Carbone et al., 1998; Orszag-Sperber et al., 1998; Giles and Goldhammer, 2000; Giles and Lawton, 2002; Alves et al., 2003; Pirazzoli et al., 2004; Bosence, 2005; Giles et al., 2008; Jaillard et al., 2013). Consequently, halokinetic sequences in carbonate environment may differ from the halokinetic sequence model proposed by Giles and Lawton (2002); Rowan et al. (2003); Giles and Rowan (2012).

This study of the Bakio diapir, in the Basque-Cantabrian basin, provides sedimentological and structural data from the exposed overburden of a diapir, where a carbonate platform and associated gravity flow on the slope (Bakio Breccias Formation) developed during Middle Albian times in response to diapir growth and adjacent mini-basin subsidence (Poprawski et al., 2014). The aims of this paper are to demonstrate that halokinetic sequences in carbonate context may differ significantly from their siliciclastic counterpart and to discuss the processes controlling carbonate-dominated halokinetic sequences. This will be achieved by addressing the following questions: (i) Where is the source for the redeposited carbonate sediments around the Bakio diapir; (ii) Which processes controlled slope stability and carbonate redeposition in the adjacent deeper depocenters; and (iii) What is the relationship between relative sea-level variations and sedimentation accumulation rates in the case of an isolated carbonate platform located on top of a passively growing diapir?

2. Halokinetic sequence models

Halokinetic sequences are defined as sedimentary succession of growth strata bounded by unconformities and thinning toward adjacent diapirs (Giles and Lawton, 2002; Rowan et al., 2003). Halokinetic sequences form due to cycles of passive diapir growth (downbuilding) followed by limited active diapir growth (active intrusion) when salt periodically pierces the diapir roof (Rowan et al., 2003) (Fig. 1a,b,c). Such sequences are controlled by drape folding and governed by the balance between the rates of diapir rise and sediment accumulation. When the velocity of diapir rise exceeds sediment accumulation rate, the diapir produces positive topography at the sea-floor and upturned strata on its flanks (Fig. 1a). Increased topographic relief may lead to erosion of the roof, sediment destabilization and redeposition. Consequently, gravity-driven deposits may accumulate on top of previously eroded and upturned strata, forming an angular unconformity (Fig. 1a). When sedimentation accumulation rate exceeds the diapir uplift velocity, the diapir becomes buried (Fig. 1b). The slope angle of the onlapping strata on the diapir-flanks decreases (Fig. 1b). Commonly, halokinetic sequences are characterized by a lower part composed of gravity-driven deposits and an upper part with fine-grained deposits (Giles and Lawton, 2002; Rowan et al., 2003). The gravity-driven deposits at the base of the halokinetic sequences commonly exhibit diapir-derived clasts showing that diapirs periodically pierces the diapir roof (Giles and Lawton, 2002; Rowan et al., 2003).

Giles and Rowan (2012) described two end-members types of halokinetic sequences: the hook halokinetic sequence and the wedge halokinetic sequence (Fig. 1d, f). Hook halokinetic sequences have high-angle unconformities (>70°), common gravity-driven deposits with rapid lateral facies variations and are associated with narrow zones of drape folding (50-200 m) (Fig. 1d). In contrast, wedge halokinetic sequences are characterized by low-angle unconformities, less common gravity-driven deposits, gradational lateral facies variations and are associated with broader zones of drape folding (300-1000 m) (Fig. 1f). Hook halokinetic sequences are thought to form when the net rate of diapir rise exceeds the net rate of sediment accumulation. Low sedimentation accumulation relative to diapir rise leads to the creation of a thin diapir roof and steep unstable diapir margins that periodically reach failure. Since the diapir roof is relatively thin, deformation is localized only near the diapir margin. Wedge halokinetic sequences are thought to form when the sediment accumulation rate exceeds the net diapir rise rate. High sedimentation accumulation relative to diapir rise leads to the creation of a thick roof. Consequently, diapir growth produces a broad deformation halo on the sea-floor and thus only gentle slope that may remain stable through time.

Hook and wedge halokinetic sequences are described to stack into tabular and tapered composite halokinetic sequences (Fig. 1e, g), respectively (Giles and Rowan, 2012). Halokinetic sequences are assumed to be scale-equivalent to parasequences sets and Composite Halokinetic Sequences (CHS) to be scale-equivalent to third order system tracts (Giles and Rowan, 2012). Tabular CHS are characterized by subparallel boundaries, thin roof and localized upturn strata localized near the diapir margin (Fig. 1e). Tapered CHS exhibit growth strata, thick roof and broad upturn strata (Fig. 1g). For diapirs located on siliciclastic-dominated shelf areas, tabular CHS commonly develop during the deposition of transgressive system tracts (TST), because sediments are restricted to the proximal areas of the shelf (Giles and Rowan, 2012). Their basal boundary commonly occurs in the early TST. Tapered CHS commonly form during the deposition of highstand system tracts (HST) and the lowstand system tracts (LST), if present, due to a high sedimentary input on the shelf (Giles and Rowan, 2012). Their basal boundary commonly occurs near the maximum flooding surface or in the early HST. In deep-water settings, creation of topographic relief and associating drape folding also occurs during low sediment accumulation phases that commonly coincide with HST, as the sedimentary input shifts toward the coastal areas (Giles and Rowan, 2012; Hearon et al., 2014b). Consequently, the boundaries of the CHS in deep-water settings commonly occur near the depositional sequences boundaries (Hearon et al., 2014b).

Among isolated carbonate platforms developed top of diapirs that were documented worldwide, only few works focus on the study of halokinetic sequences in carbonate settings (Giles and Lawton, 2002; Rowan et al., 2003; Giles and Rowan, 2012; Kernen et al., 2012; Hearon et al., 2014a, 2015). In the mixed carbonate-siliciclastic system of the La Popa basin, Giles and Lawton (2002); Rowan et al. (2003) described carbonate lentils made of shallow-water limestones and submarine carbonate debris flows, thinning away from the diapirs. These lentils range from 400 m to 5 km in length and from 10 m to 160 m in thickness and are interpreted as the result of carbonate platform growth on top of the diapir. Giles and Lawton (2002); Rowan et al. (2003) showed that these carbonate sediment accumulation mainly developed during transgressive system tracts, due to the retrogradation of the siliciclastic facies, toward the shoreline. These carbonates develop during low siliciclastic accumulation on top of the diapir combined with drape folding and creation of topographic relief. Therefore, they developed above the unconformities at the base of the halokinetic sequences. In the same area, Giles and Rowan (2012) hypothesized that carbonate-dominated CHS tend to be preferentially tapered even when the sediment accumulation is low, due to the creation of thick diapir roof where the carbonate platform grew. This hypothesis is corroborated by the work of Kernen et al. (2012); Hearon et al. (2014a, 2015), in the Central Flinders and in the Willouran ranges, in Australia, where they described mainly carbonate-dominated tapered CHS.

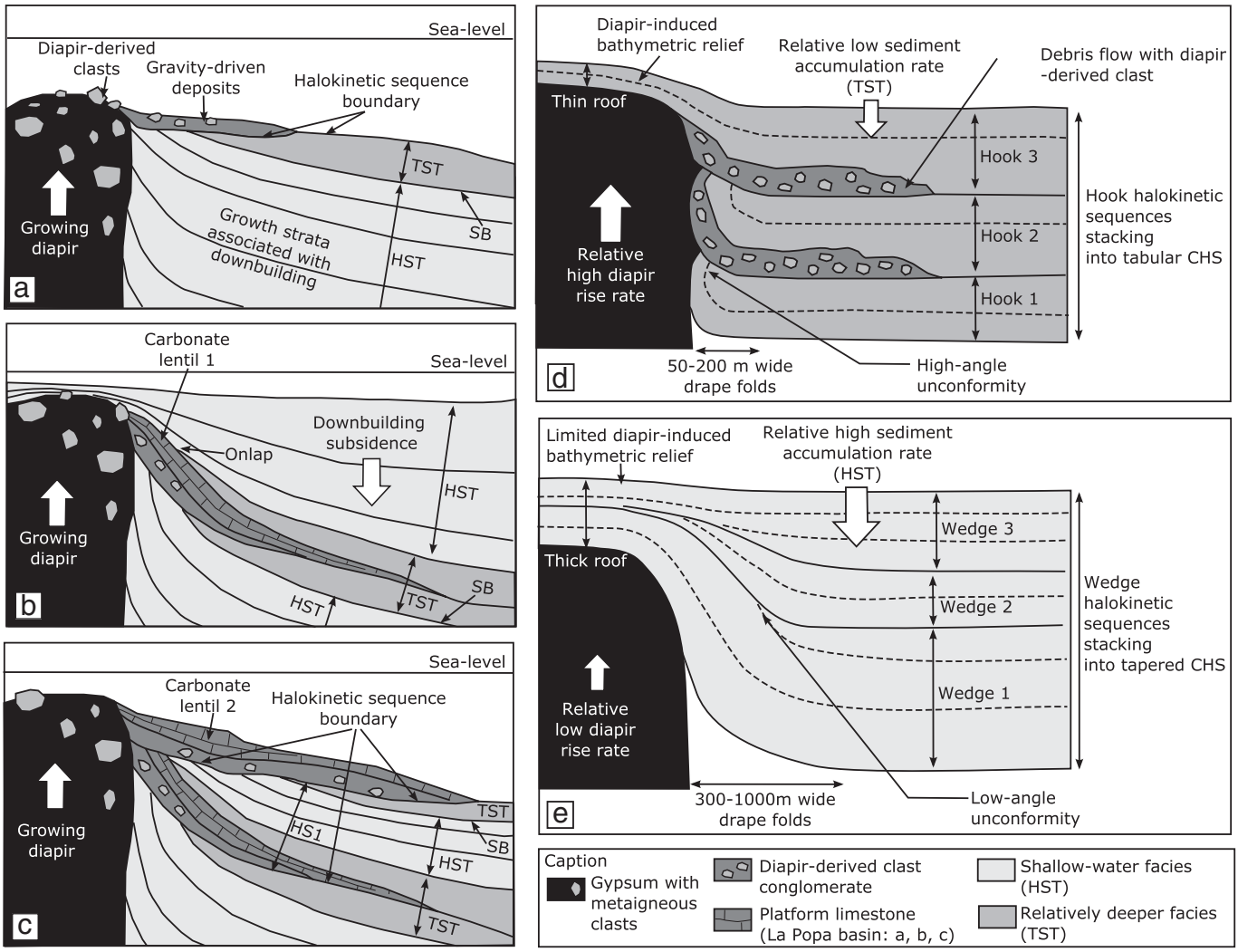

Fig. 1. Halokinetic sequence model from the La Popa basin (a., b. & c.), from Giles and Lawton (2002) and hook and wedge halokinetic sequence associated with the tabular and tapered Composite Halokinetic Sequences (CHS) models (d.& e.), from Giles and Rowan (2012). When diapir rise velocity overcomes sediment accumulation, diapir growth produces positive surface relief and upturned strata, leading to sediment sliding and redeposition of gravity-driven deposits top of an angular unconformity (a.). When sediment accumulation overcome the diapir growth velocity, the diapir is buried and sediment laps on the diapir flanks that remain stable (b.). Repetition of phase a. leads to the creation of a new halokinetic sequence (c.). Giles and Lawton (2002) initially proposed that halokinetic sequences are at the scale of 3rd order systems tracts (a,b&c). However, the recent work of Giles and Rowan (2012) suggest that halokinetic sequences stack into composite halokinetic sequences, which are currently considered to be at the scale of the 3rd order systems tracts (d &e). Hook halokinetic sequences have high-angle unconformities and common gravity-driven deposits with rapid facies variations and narrow zones of drape folding and stack into tabular composite halokinetic sequences (d.). They commonly form during transgressive system tracts, for diapir in the shelf, due to the low sediment accumulation rates (d.). Wedge halokinetic sequences are characterized by low-angle unconformities, less common gravity-driven deposits, gradational facies variations and broad zone of drape folding and stack into tapered composite halokinetic sequences (e.). They commonly form during highstand system tracts, for diapir in the shelf, due to the high sediment accumulation rates (e.).

3. Geological setting

3.1. Mesozoic and Tertiary history of the Basque-Cantabrian Basin

The Basque-Cantabrian basin is an inverted rift, located in northern Spain (Fig. 2a), in the westernmost part of the Pyrenees (Gómez et al., 2002; Ferrer et al., 2008). The opening of this basin is related to the rotation of the Iberian plate during the Cretaceous (García-Mondéjar et al., 1996; Martín-Chivelet et al., 2002).

Triassic gypsum and red clays corresponds to the oldest Mesozoic deposits of the Basque-Cantabrian basin. These rocks are exposed in several diapirs (Fig. 2a) that were growing during Albian (e.g. López-Horgue et al., 2010; Quintà et al., 2012; Poprawski et al., 2014). Jurassic to Early Albian strata correspond to thin, fluvial, alluvial and shallow marine rocks (García-Mondéjar et al., 1996, 2004; Martín-Chivelet et al., 2002). Middle Albian to Cenomanian units are characterized by deep-water siliciclastic turbidites and redeposited carbonate, regionally called the Black Flysch units (García-Mondéjar et al., 1996, 2004; Martín-Chivelet et al., 2002), that were deposited in the main depocenter, called the Basque Trough (Fig. 2b). The development of the Black Flysch units resulted from a combination of (1) subsidence-driven deepening of the Basque Trough from Aptian to Turonian times (Gómez et al., 2002; García-Mondéjar et al., 2005) and (2) global sea-level rise during the Early Albian (Vail et al., 1977; Haq et al., 1987; Brunet, 1997; De Graciansky, 1998). Subsidence in the Basque Trough was coeval with the uplift of the Landes Massif, which is a basement block (Fig. 2), presently located offshore (Gómez et al., 2002; Ferrer et al., 2008). This basement block is considered as the source area for the siliciclastic units of the Black Flysch group (Voort, 1964; Rat, 1988; Robles et al., 1988; García-Mondéjar et al., 1996; Agirrezabala, 1996; Martín-Chivelet et al., 2002). From Late Cenomanian to Early Campanian, the Basque Trough remained subsiding and filled by calcareous fine-grained turbidites and marls, locally called the Plenzia Formation. (Mathey 1987; Castañares et al., 2001; Martín-Chivelet et al., 2002).

Inversion of the Basque-Cantabrian basin started from Late Cretaceous (Campanian) and culminated during Eocene (Gómez et al.,

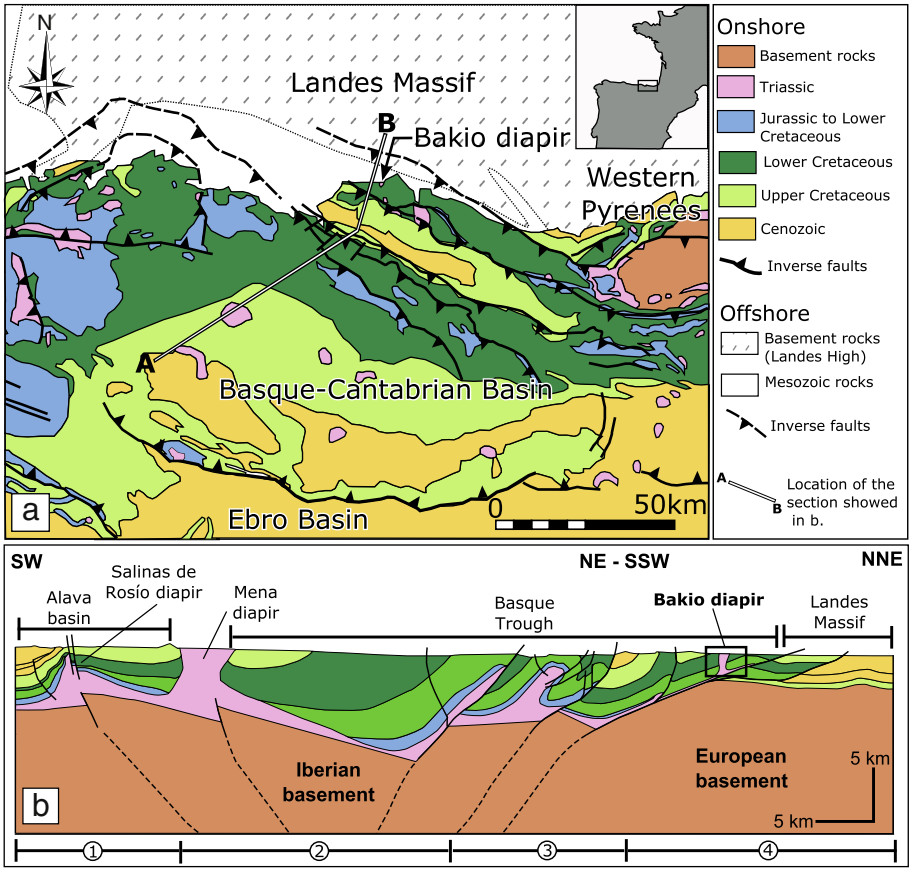

Fig. 2. a. Geological map of the Basque-Cantabrian basin, modified from García-Mondéjar et al. (1996) for onshore areas and from Roca et al. (2011) for offshore areas. b. Composite structural cross-section of the Basque-Cantabrian basin built using the cross-sections of Hernaiz-Huerta and Solé Pont (2000) for domain 1, Serrano and Martínez del Olmo (1989) for domain 2, Garrote et al. (1995) for domain 3 and Gómez et al. (2002) for domain 4. The Bakio diapir has been added, modifying the structural cross-section of Gómez et al. (2002). The Bakio diapir is located on the northern margin of the Basque Trough, which belong to the European plate during Cretaceous. Basement geometries are hypothetic.

2002). A limited shortening, from 40 to 50 km, has been assumed by Ábalos et al. (2008) and thus, several Cretaceous structures, such as the Bakio diapir (Poprawski et al., 2014) have been preserved or only slightly reactivated in the Basque-Cantabrian basin.

3.2. Stratigraphy of overburden of the Bakio diapir

The Bakio diapir is composed of Triassic red clays and gypsum. Early to Late Albian overburden includes six stratigraphic units (Figs. 3, 4). The Bakio marls unit and the Bakio Breccias Formation correspond to the youngest carbonated deposits in the area (early Middle Albian). The overlying Sollube, Cabo Matxitxako, Punta de Bakio and Jata units correspond to the oldest units of the Black Flysch Group (early Late Albian and Late Albian) in the area.

The Bakio marls unit is only exposed on the eastern flank of the Bakio diapir (Figs. 3, 4) and its base it not exposed. The minimal thickness of the exposed Bakio marls unit is 60 m. This unit consists of interbedded marls and thin-bedded packstones, interpreted as deposited in an outer shelf setting (García-Mondéjar and Robador, 1987; Robles et al., 1988). The Bakio Breccias Formation, composed of carbonate breccias interbedded with marls (García-Mondéjar and Robador, 1987; Robles et al., 1988) is unconformably overlying the Bakio marls unit in the eastern flank (Fig. 4). This unit is 550 m thick in the eastern flank, and 205 m thick in the western flank, where its base is not exposed (Fig. 4). In the eastern flank of the diapir, two distinct units are present above the Bakio Breccias Formation: the Sollube and the Cabo Matxitxako units (Figs. 3, 4). The Sollube unit is made of thin-bedded, fine-grained siliciclastic turbidites interbedded with marls (Vicente-Bravo and Robles, 1991a) and is about 150 m thick in the northern part of the eastern flank of the diapir. This unit is thickening southward to a maximum of 1600 m (Vicente-Bravo and Robles, 1991a). The Cabo Matxitxako unit consists of amalgamated, thick-bedded, coarse-grained siliciclastic turbidites (Robles et al., 1988) and is about 50 m thick. In the western flank of the diapir, two distinct units are found above the Bakio Breccias Formation: the Punta de Bakio and the Jata units (Figs. 3, 4). The Punta de Bakio unit is composed of marl interbedded with thin-bedded, fine-grained siliciclastic turbidites, and with matrix-supported breccias (Robles et al., 1988; Poprawski et al., 2014). This unit is about 60 m thick near the diapir and is thickening away from the diapir (Poprawski et al., 2014). The Jata unit consists of marls alternating with fine-grained to coarse-grained siliciclastic turbidites with slumps and breccia deposits (Vicente-Bravo and Robles, 1991b). This unit is 660 m thick (Robles et al., 1988). The Sollube and Cabo Matxitxako units are present only east of the diapir, while the Punta de Bakio and Jata units are present only west of the diapir (Figs. 3, 4).

Complex lateral facies variations and sparse biostratigraphic data make difficult correlations between units from either flank of the Bakio diapir (Figs. 3, 4). According to the available data (Wiedmann and Boess, 1984; García-Mondéjar and Robador, 1987; Robles et al., 1988; López-Horgue et al., 2009), the Bakio Breccias Formation is early Middle Albian in age. The underlying Bakio marls unit have yet to be dated, but is probably of Early Albian age, as it is overlain by the Bakio Breccias Formation (García-Mondéjar and Robador, 1987; Robles et al., 1988). The units of the Black Flysch Group are of Middle to Early Cenomanian in age (Robles et al., 1988; Vicente-Bravo and Robles, 1991a and b). The Punta de Bakio unit and the Sollube unit are early Late Albian and Late Albian in age, respectively. López-Horgue et al. (2009) dated the Jata unit as early Middle Albian, in Armintza (7 km

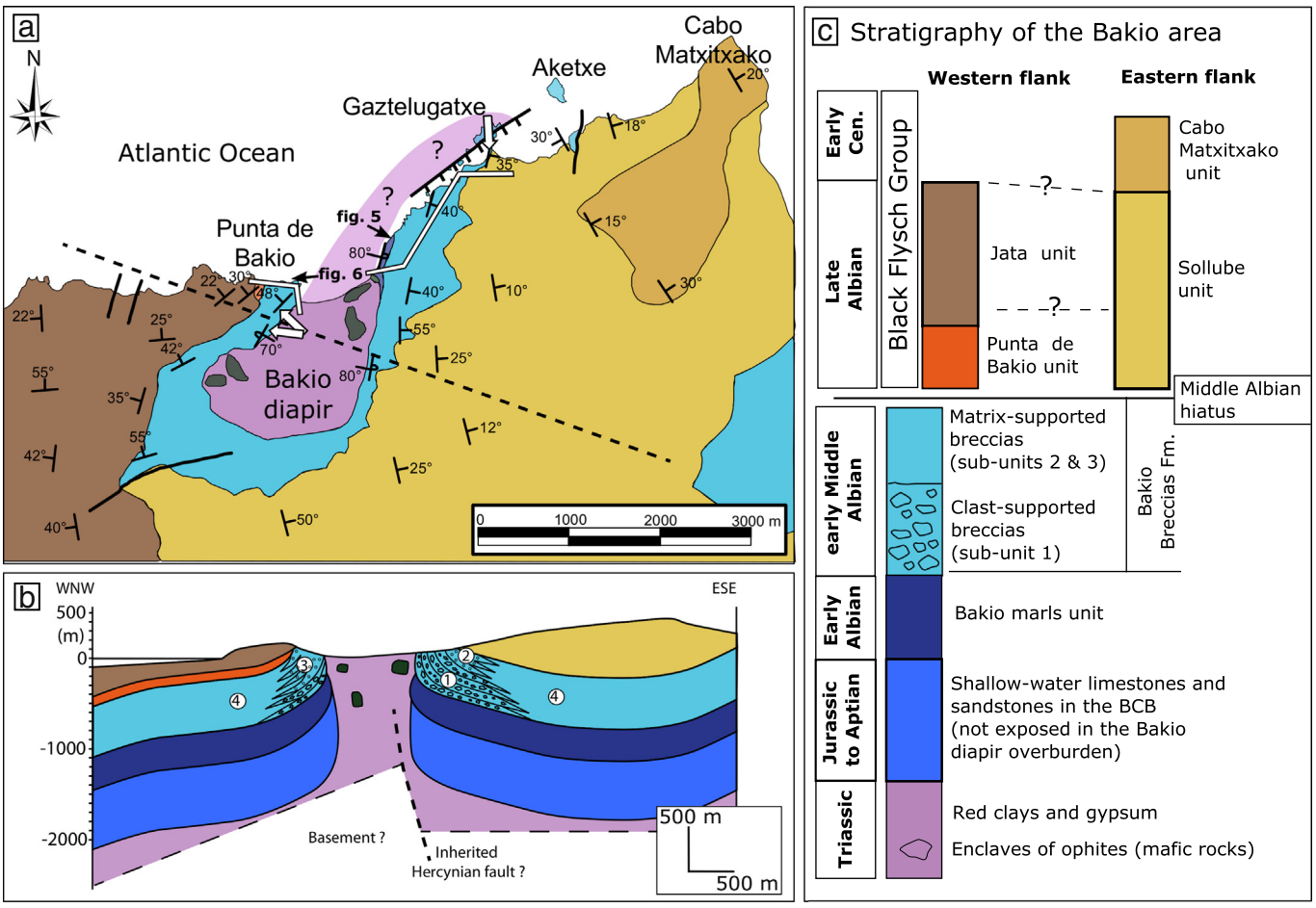

Fig. 3. a. Geologic map of the Bakio area based on new field work and data from Robles et al. (1988, 1989); Pujalte et al. (1986); García-Mondéjar and Robador (1987); Vicente-Bravo and Robles (1991a, 1991b); Poprawski et al. (2014). The white lines show the location of the exposures used to build the stratigraphic sections presented on Fig. 4. The white arrows represent the slumping directions deduced from Poprawski et al. (2014). The light pink colour represents the possible extension of the salt, below the Gaztelugatxe escarpment, according to the interpretation of Poprawski et al. (2014). Location of Figs. 5, 6 is also indicated. b. Structural cross-section through the Bakio diapir and its overburden. In the eastern flank, the lower and upper parts of the Bakio Breccias Formation are called sub-unit 1 (1) and sub-unit 2 (2), respectively. In the western flank, a third sub-unit (3) is exposed and is probably time-equivalent with sub-unit 2. However, it is not possible to decipher from the biostratigraphic data whether the base of sub-unit 3 falls laterally inside sub-units 1 or 2. In the southern part of the diapir, where outcrops are scarce, the Bakio Breccias Formation display mainly marly facies and relatively finer-grained facies compared to the north (4). c. Schematic stratigraphic section of the Bakio area from Triassic to Early Cenomanian, using data from Robles et al. (1988, 1989); Pujalte et al. (1986); García-Mondéjar and Robador (1987); Vicente-Bravo and Robles (1991a, 1991b). BCB: Basque-Cantabrian basin.

west of Bakio), while it overlies the Punta de Bakio unit (early Late Albian) in the western flank of the Bakio diapir. The Cabo Matxitxako unit is probably Late Albian or Early Cenomanian in age because it is overlying the Sollube unit (Late Albian).

4. Sedimentary and structural data

4.1. Facies description and interpretation

4.1.1. Siderite layers

Fine-grained, thin-bedded calcarenites layers with diagenetic red mineralization of siderite are found in the Bakio Breccias Formation (Fig. 7a). Slumps including folded siderite and breccia layers with siderite pebbles indicate an early development of diagenetic siderite in poorly consolidated sediments. Such siderite layers have been already described in the Black Flysch Group (Badillo et al., 1983; Robador and Garca-Mondéjar, 1987; Chaler et al., 2005), as well as in the Jata and Armintza units (Ábalos and Elorza, 2012), few kilometers west of Bakio. According to Ábalos and Elorza (2012), diagenetic siderite nodules, layers and concretions (Fig. 7a) are frequently cementing fine-grained turbidite usually the Td-e terms of Bouma sequences (Bouma, 1962). Consequently, in the Bakio breccias Formation, siderites layer are interpreted as diagenetic siderite cementing fine-grained calcareous turbidites.

4.1.2. Coarse-grained calcarenite deposits (type 1-calcarenite)

The first type of calcarenite corresponds to massive or laminated coarse-grained calcareous sand, mainly found on top of clast-supported breccia beds (Fig. 7b). Clast-supported breccia and type 1-calcarenite form normally graded beds. The vertical change from clast-supported breccia to type 1-calcarenite is often transitional without sharp contact, suggesting a single depositional event. Clast-supported breccia beds often display planar tops as calcarenite drapes the underlying blocks. These features indicate that coarse-grained calcarenite deposits may result of grain flows (sensus Talling et al., 2012) deposited just after clast-supported breccia probably by the same depositional event.

4.1.3. Medium to fine-grained calcarenite deposits (type 2-calcarenite)

The second type of calcarenite corresponds to fine- to medium-grained calcareous sands with basal scours, planar, oblique and convolute laminations, commonly interbedded with marls (Fig. 7c, d). They are often normally graded, with calcirudite deposits at the base, which may also exhibit rare flute casts and water escape structures (Fig. 8a). These calcarenite beds exhibit features similar to the Ta-c terms of the

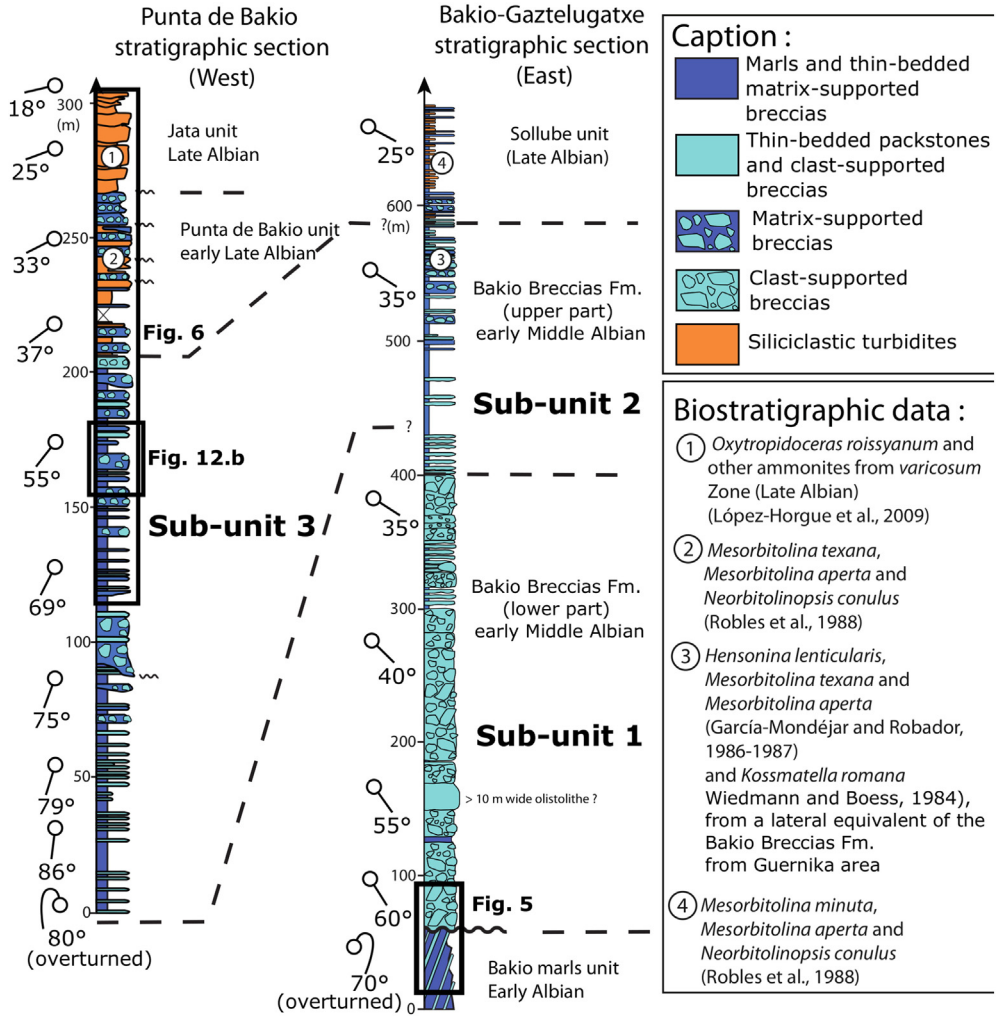

Fig. 4. Stratigraphic sections on both flanks of the Bakio diapir (modified from Poprawski et al., 2014) and their possible correlations based on biostratigraphic data from previous works of Wiedmann and Boess (1984); García-Mondéjar and Robador (1987); Robles et al. (1988); López-Horgue et al. (2009). These sections have been built only from the outcrops in the current coastline (Fig. 3a) since exposures inland are scarce due to the vegetation. Sub-units 2 and 3 are probably time-equivalent, since they display similar facies and since they are both located below the Black Flsych Group units (Punta de Bakio unit to the west and Sollube unit to the east). The Punta de Bakio and Jata units (Black Flsych Group) are probably the lateral equivalent of the Sollube unit.

Bouma sequence (Figs. 7c, d, 8a), and thus may be interpreted as fine-grained carbonate turbidites resulting of high- to low-density turbidity current (sensus Talling et al., 2012).

4.1.4. Calcirudite deposits

Calcirudite layers consist of limestone gravels (from 0.2 to 5 centimeters), bioclasts from rudistids, corals, regular urchin spines, brachiopods, bryozoans, various bivalves and entire fossils as orbitolinids (Fig. 8b) and are either normally graded, or massive. They are often located at the base of fine to medium-grained calcarenite deposits with planar laminations (Fig. 7c) and exhibit basal scours and rare water escape structures (Fig. 8c). These features indicate that calcirudite deposits be interpreted as the result of gravel flows or high-density turbiditiy currents (sensus Talling et al., 2012) coming directly from an unlithified platform.

4.1.5. Clast-supported breccia deposits (clast-supported breccia)

The clast-supported breccia layers are composed of angular limestone blocks, mainly floatstone and rarely mudstone, with a clast-supported texture, without matrix (Figs. 8d, 9a) and are commonly massive and normally graded, with common erosive bases. Beds are tabular and range from 10 cm to 10 m in thickness (Figs. 8d, 9a). Floatstone blocks that commonly display entire or fragmented rudistid and coral fossils, are commonly up to 2 meters in diameter (Figs. 8d, 9d) and often deform underlying marls. Some beds exhibit a transitional contact from matrix- to clast-supported breccia, and an upward increase of blocks relatively to the amount of matrix (Fig. 10b). The top of these beds is composed of clast-supported breccias with limestone blocks, reworked siderite pebbles, and locally some marly matrix clasts (Fig. 9b, c). Locally, these beds are inversely graded with larger blocks at the top. Some of these clast-supported breccia beds are channelized and interbedded with marls (Fig. 9c). The size of the blocks and the clast-supported texture suggests that the clast-supported breccia deposited as non-cohesive debris flows or rock fall (sensus Talling et al., 2012).

4.1.6. Matrix-supported breccia deposits (matrix-supported breccia)

Matrix-supported breccia layers consist of heterogeneous angular blocks in a marly matrix (Fig. 9d) and are either normally or inversely graded. The matrix consists of marl, or mixed marl, limestone debris and skeletal grains (crinoids, regular urchin spines, orbitolinids, fragments of bivalves, brachiopods, rudistids, bryozoans and corals). Clasts consist of block of floatstone with rudistid and coral fossils, rare blocks of mudstone and clast-supported breccia, siderite pebbles and slumped beds (slumped siderite, coarse-grained calcarenite and clast-supported

breccia beds). The normally graded beds often display erosive bases, and deformation of the underlying marl below the larger blocks is often observed. The inversely graded beds commonly exhibit planar bases and irregular tops, due to large blocks floating at the top of the bed (Fig. 9b, c). Plastic deformation and the abundance of marly matrix indicate that matrix-supported breccia beds may result from high strength cohesive debris flows (sensus Talling et al., 2012).

4.1.7. Slumps

Slumped beds show soft sediment deformation with folded calcarenite beds (Fig. 10d), or folded breccia beds, included in a marly matrix, often containing skeletal grains (crinoids, regular urchin spines, orbitolinids, fragments of bivalves, brachiopods, rudistids, bryozoans and corals). At the toe of the Gaztelugatxe escarpment (upper part of the Bakio Breccias Formation, sub-unit 2), a 5.5 m thick bed laterally evolves from slump to matrix-supported breccia (Fig. 10c). In the proximal part, near the Gaztelugatxe escarpment, this bed is composed of large blocks of floatstone with rudistid and coral fossils associated with slumped beds of clast-supported breccia and coarse-grained calcarenite floating in a marly matrix. The base of this bed is a sliding scar, which truncates laterally some beds of coarse-grained calcarenite and clast-supported breccia interbedded with marls. This bed grades downslope to matrix-supported breccia.

4.2. Units in the Bakio Breccias Formation

The Bakio Breccias Formation on both flanks of the diapir is mainly exposed along the coastline and the exposures inland are scarce due to the vegetation cover. The following description mainly focuses on the vertical architecture of the Bakio Breccias Formation, from the exposures in the coastline (Fig. 3). This unit is divided into three different sub-units. In the eastern flank, a lower clast-dominated sub-unit (sub-unit 1, from 60 to 428 m, in Fig. 4) and an upper mud-dominated sub-unit (sub-unit 2, from 428 to 585 m, in Fig. 4) are exposed. The base of sub-unit 1 consists of an angular unconformity developed top of the Bakio marls unit (Fig. 5). In the western flank, a third mud-dominate sub-unit is exposed (sub-unit 3, from 0 to 205 m, in Fig. 4) and is involved in a growth strata (Fig. 6). Even if sub-units 2 and 3 display similar facies and are probably time-equivalent (Fig. 4), it is not possible to distinguish from the biostratigraphic data whether the base of sub-unit 3 falls laterally inside sub-unit 1 or sub-unit 2, and thus sub-units 2 and 3 are considered as distinct units. In the southern part of the diapir, where outcrops are scarce, the Bakio Breccias Formation display mainly marly facies and relatively finer-grained facies compared to the north.

Sub-unit 1 is clast-dominated and consists of thick clast-supported breccia beds (from 1 to 10 m thick) with large blocks (up to 2 m in diameter) of floatstone with rudistid and coral fossils. The blocks are stacked together or interbedded with thin-bedded calcarenite and marly intervals (Fig. 4). Thin intervals of marl (few centimeters thick) are locally present at the base of the beds and are deformed by the overlying blocks. Massive or laminated calcarenite layers drape the top of clast-supported breccia beds, with a transitional contact. Sub-unit 1 displays a succession of sequences with thin marl beds at the base, overlain by thick ortobreccia layers, and capped by thin-bedded calcarenite. The upper part of sub-unit 1 displays thinning and finning upward features (Fig. 4).

Sub-units 2 and 3 are mud-dominated and are composed of thick matrix-supported breccia beds (20 cm to 3 m thick), alternating with thick marly intervals (1 to 20 m thick) and thin-bedded calcarenite, calcirudite and clast-supported breccias (Fig. 4). Blocks within matrix-supported breccia can reach up to 3 meters in diameter. Clast-supported breccia levels are thin-bedded and display smaller blocks from 1 to 30 cm in diameter, compared to the clast-supported breccia beds of sub-unit 1. Some clast-supported breccia beds are channelized and intercalated within marls. Fine to medium-grained calcarenite beds have basal scours, planar, oblique and convolute laminations, and are interbedded with marl. Some slumped intervals include limestone blocks and slumped clast-supported breccias and calcarenite beds within a marly matrix. In sub-units 2 and 3, there is no apparent organisation in the vertical facies succession (Fig. 4).

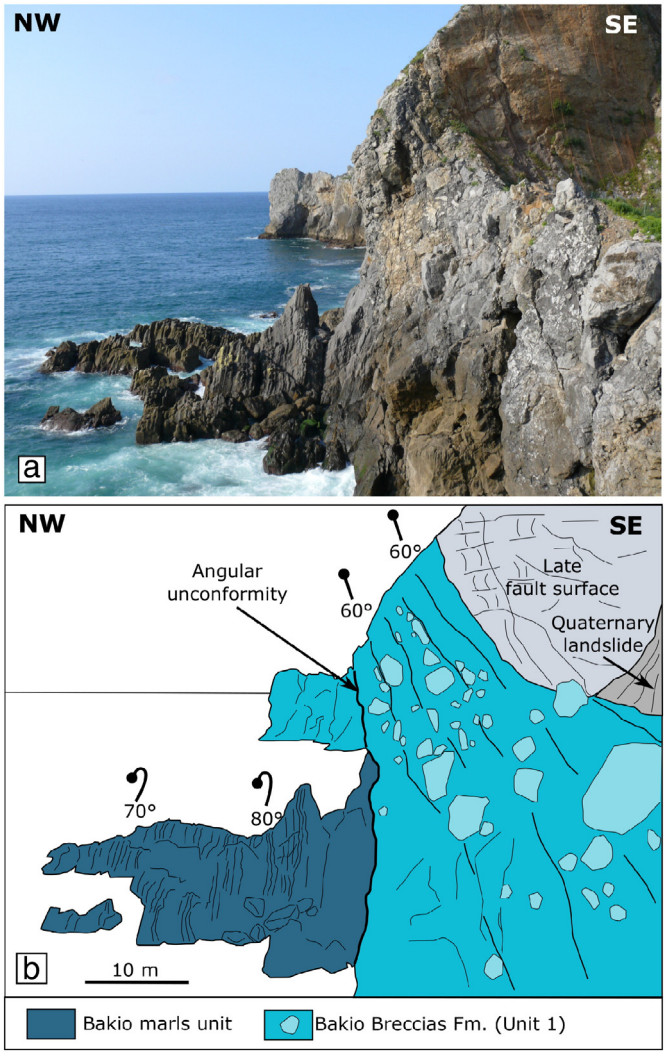

Fig. 5. a. View of the eastern flank of the Bakio diapir, where the base of the Bakio Breccias Formation (sub-unit 1) is cropping out (location Figs. 2, 3). b. Interpretation of the outcrop showing that the Bakio Breccias Formation is unconformably overlying the overturned Bakio marls unit.

4.3. Structures in the diapir flanks

On the northern part of the eastern flank of the Bakio diapir, the Bakio Breccias Formation (sub-unit 1) is unconformably overlying the Bakio marls unit (Figs. 4, 5). Below the unconformity, bedding planes in the Bakio marls unit are overturned and dipping 80° toward the NW (Figs. 4, 5). The first bedding planes in the Bakio Breccias Formation above the unconformity are dipping 60° toward the SE, forming a high angle unconformity, with an angle up to 40° (Figs. 4, 5). Above the unconformity, the Bakio Breccias Formation forms a growth strata with a total angle between the most and less dipping beds reaching 25° and mainly occurring in sub-unit 1 (Fig. 4). On the southern part of the eastern flank, mapping reveals also a growth strata with a total angle between the most and less dipping beds reaching 45° in the Bakio Breccias Formation (Fig. 3a).

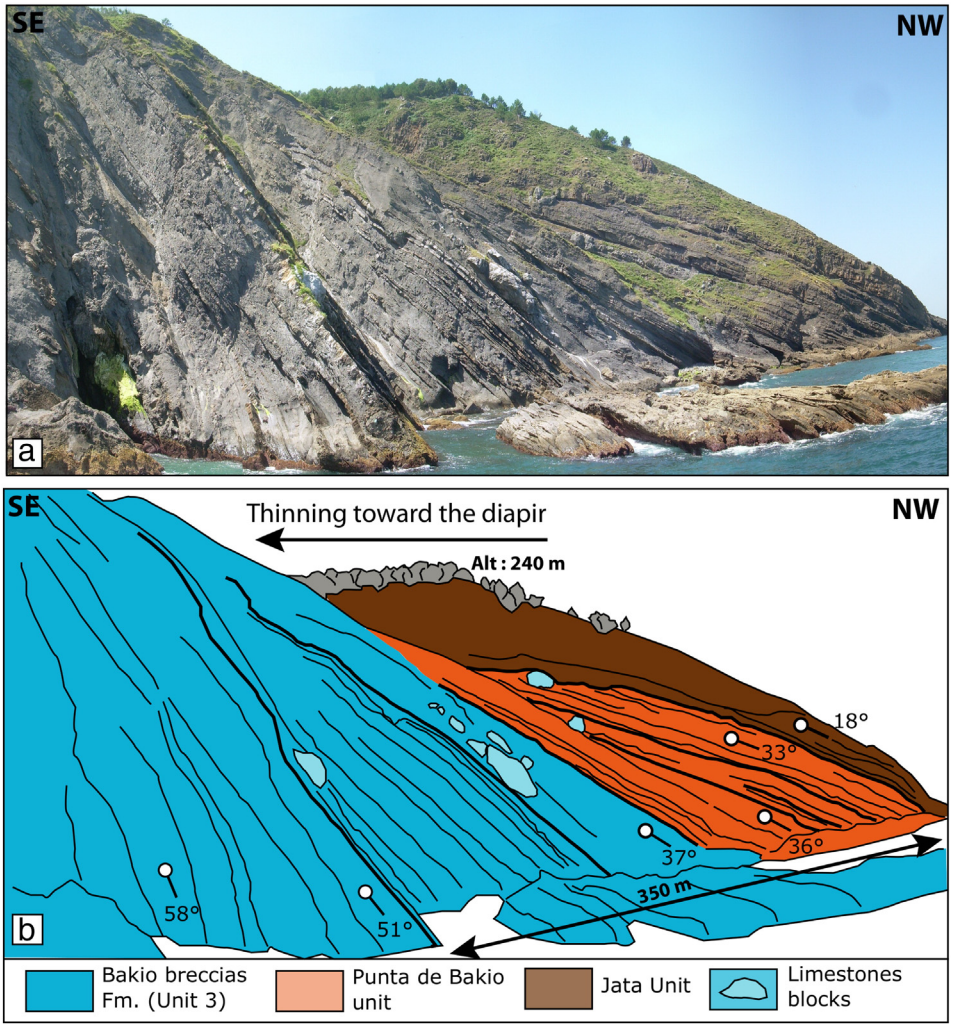

Fig. 6. a. Westward view of the Punta de Bakio sedimentary growth strata (modified from Poprawski et al., 2014; location Figs. 2, 3). b. Interpretation of the growth strata, composed from bottom to top of the Bakio Breccias Formation, the Punta de Bakio and the Jata unit. These units exhibit an increase of the bedding dip angle toward the diapir and the Punta de Bakio unit displays four angular unconformities. Beds are overturned near the diapir contact (about 10 m, right of the picture).

The western flank displays well-exposed growth strata with overturned to horizontal beds and several angular unconformities (Fig. 6) (Arbués et al., 2012; Rowan et al., 2012b; Poprawski et al., 2014; Ferrer et al., 2014). From east to west (Fig. 6), the growth strata are composed of the Bakio Breccias Formation (Middle Albian), Punta de Bakio (early Late Albian) and Jata units (Late Albian) (Poprawski et al., 2014). The Punta de Bakio unit shows several angular unconformities, including its top (Fig. 6b). All units thin and are upturned toward the diapir. Beds are dipping 80° toward the SE (overturned strata) to 20° toward the NW, in the upper part of the Bakio Breccias Formation and in the uppermost part of the Punta de Bakio unit, respectively (Poprawski et al., 2014) (Figs. 4, 6b). The total angle between the most and less dipping beds reaches 63° in the Bakio Breccias Formation. The Jata unit is horizontal on the coastline, about 700 m away from the diapir contact (Rowan et al., 2012b; Poprawski et al., 2014; Ferrer et al., 2014). Associated with the growth strata and the unconformities, several slumped structures have been described on both flanks of the diapir (Poprawski et al., 2014).

A vertical and irregular escarpment developed in the lower part of the Bakio Breccias Formation on the Gaztelugatxe Island (Fig. 3a), about 1 km NE of the Bakio diapir (Poprawski et al., 2014). It strikes NE–SW at present (N048°, 90°). Mapping suggests that the upper part of the Bakio Breccias Formation pinches out northward and onlap on the scarp (Poprawski et al., 2014). The orientations of the escarpment and of the Bakio diapir (Fig. 3a) suggest that both structures are connected in the subsurface (Poprawski et al., 2014).

5. Sedimentary and structural analyses

5.1. Environments of deposition

5.1.1. Clast-supported breccia deposits

In sub-unit 1, the presence of rudistids and corals in the blocks suggests a source from a lithified platform margin, as rudistids-corals assemblage commonly produce reef or isolated buildups at the platform margin (e.g. Pomar and Hallock, 2008; Skelton and Gili, 2012). In addition, the size and angular shape of blocks (Fig. 8d) demonstrate a short transport from the source and the absence of distal feature suggests a relatively proximal environment. Therefore, clast-supported breccia beds are interpreted to result of non-cohesive debris flows or rock fall (sensus Talling et al., 2012) deposited at the toe of a steep platform margin, in the upper slope, similarly to other carbonate systems worldwide (e.g. Mullins and Cook, 1986; Spence and Tucker, 1997; Drzewiecki and Simó, 2002; Bahamonde et al., 2004; Hüneke and Krienke, 2004; Emmerich et al., 2005; Verwer et al., 2009; Playton et al., 2010; Mulder et al., 2012a, 2012b) or in the Basque-Cantabrian basin (García-Mondéjar and Fernández-Mendiola, 1993; Rosales, 1999; Gómez-Pérez et al., 1999; Fernández-Mendiola et al., 2013).

5.1.2. Coarse-grained calcarenite deposits (type 1-calcarenite)

Clast-supported breccia beds are often draped by calcarenite layers with a transitional contact (Figs. 7b, 9a), suggesting that rock falls

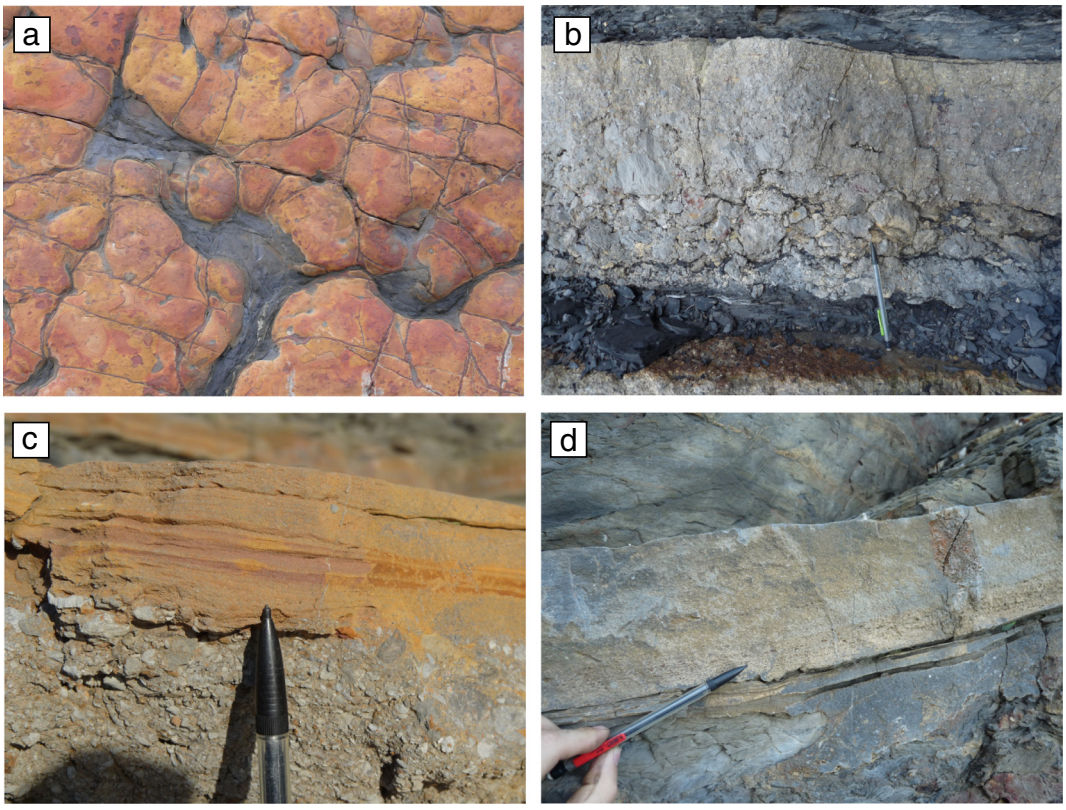

Fig. 7. Pictures of siderite and calcarenite layers. a. View of the top of a siderite layer. b. Single bed with a normal grading showing a transitional vertical change from clast-supported breccia to calcarenite. c. Laminated calcarenite overlying an interval of calcirudite. d. Fine to medium-grained calcarenite with basal scours and planar laminations, interbedded with marls.

were followed by the deposition of calcarenite beds, as a single gravitational event. Mullins and Cook (1986); Loucks et al. (2011) demonstrated the same relationship between calcarenite layers and clast-supported limestone conglomerates. Coarse-grained calcarenite may be interpreted as the result of grain flows deposited above rock falls deposits, and generated by the same sliding event. Consequently, they can be considered as a proximal facies, also deposited at the toe of the platform margin, in the upper slope.

5.1.3. Slumps

The slumped beds made of folded calcarenite (Fig. 10d) and clast-supported breccia (Fig. 10c) suggests a post-depositional reworking by slope instabilities of the facies previously deposited by grain flows and rock falls in the upper slope, while the matrix is derived from marls previously deposited as suspension fallout, in relatively distal areas (e.g. Flügel, 2004; Tucker and Wright, 2009). Such mixed sediments indicate a reworking from different sources during slumping and reveal a transport over relatively long distance, able to sample these various sediments, as demonstrated by Mullins and Cook (1986). Therefore, slumps are interpreted to be source from the upper slope, reworking previously deposited facies and clasts (clast-supported breccia, calcarenite and skeletal grains) and to be deposited in the lower slope.

5.1.4. Matrix-supported breccia deposits

Blocks, debris and matrix are similar in slumps and matrix-supported breccia (Figs. 9d, 10c) and there is a clear example of a slump, which grades laterally to matrix-supported breccia (Fig. 10c). Moreover, several matrix-supported breccia beds include small slumped beds. This suggests that slumps are parent deposits of matrix-supported breccia and are thus genetically linked. Slumping is interpreted as the initial gravity-driven process able to create matrix-supported breccia by down-slope flow transformation. Plastic deformation in slumped layers and the abundance of marly matrix indicate that matrix-supported breccia beds result from high strength cohesive debris flows (sensus Talling et al., 2012), deposited in the lower slope, similarly to other carbonate systems (e.g. Mullins and Cook, 1986).

5.1.5. Siderite layers

According to Ábalos and Elorza (2012), diagenetic siderite nodules, layers and concretions (Fig. 7a) occur frequently in abyssal plain facies, cementing fine-grained turbidites and often indicate condensed periods during sediment starvation stage. In the Bakio area, siderite layers commonly occur inside relatively thick marly intervals, supporting the hypothesis of relatively distal facies.

5.1.6. Siderite-bearing clast-supported breccia deposits

Clast-supported breccia layers with siderite pebbles and local marly matrix (Fig. 9b,c) correspond to relatively distal facies as they rework siderite layers, interpreted as fine-grained turbidites (Ábalos and Elorza, 2012). Siderite pebbles may be considered as rip-up mud clasts, since siderite formation occurred in poorly lithified sediments (Ábalos and Elorza, 2012). Clast-supported breccia with siderite pebbles is often found either on top of matrix-supported breccia beds with gradational contact, suggesting a flow transformation from matrix- to clast-supported breccia, as already documented by Mullins and Cook (1986). Consequently, siderite-bearing clast-supported breccias may be interpreted as hyperconcentrated flows, derived from the matrix-supported breccia beds considered as the parent deposit.

5.1.7. Calcirudite deposits

In calcirudite (Figs. 7c, 8b), the occurrence of allochems and limestone gravels points to an unlithified source (e.g. Mullins and Neuman, 1979; Mullins et al., 1984; Grammer et al., 1993; Franseen et al., 1998; Drzewiecki and Simó, 2002; Payros and Pujalte, 2008; Janson et al., 2011; Goldstein et al., 2012). The presence of orbitolinids suggests

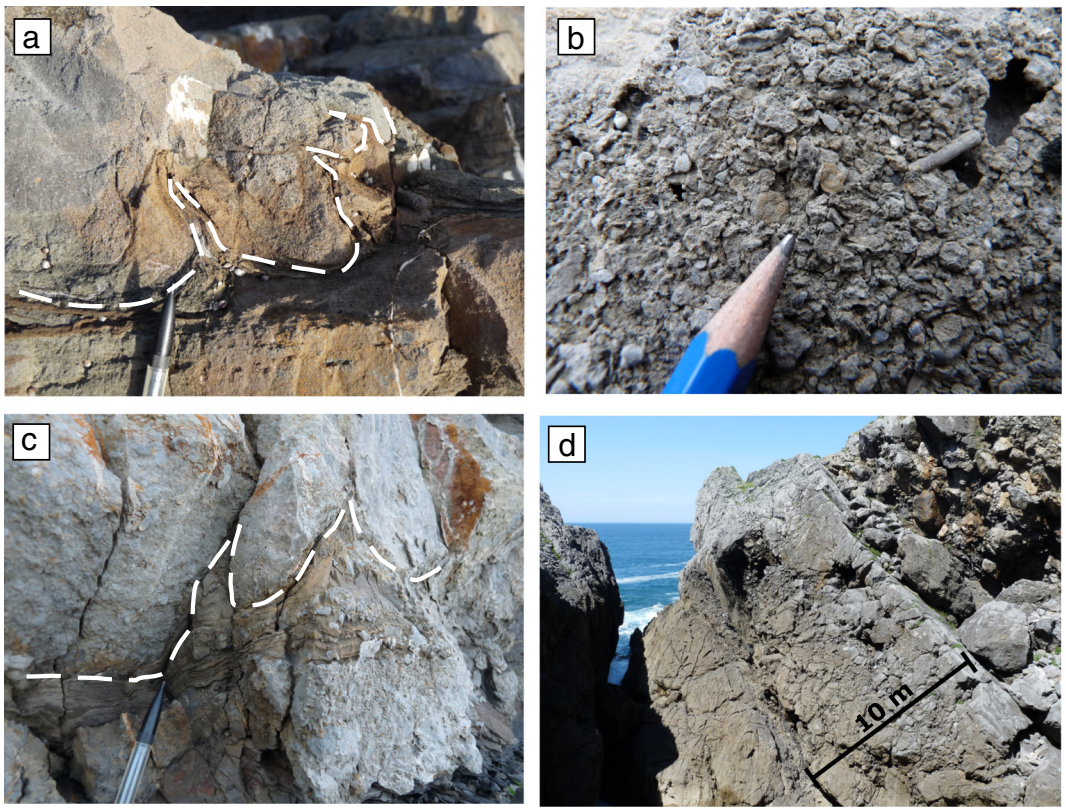

Fig. 8. Pictures of calcarenite, calcirudite and clast-supported breccia layers. a. Calcarenite with water-escape structures. b. Details of a calcirudite illustrating the variability of clasts with limestone gravels and bioclasts (here, regular urchin spines and *Orbitolines*). c. Calcirudite with water-escape structures. d. Thick beds of clast-supported breccia (up to 10 m), with large olistoliths (here up to 5 m long).

that these facies were sourced from internal areas of an unlithified platform, since orbitolinids in several Albian platforms of the Basque-Cantabrian basin are commonly found in such environments (García-Mondéjar and Fernández-Mendiola, 1993; Rosales, 1999; Gómez-Pérez et al., 1999; Fernández-Mendiola et al., 2013). However, calcirudite beds are mainly found interbedded with distal facies like marls, suggesting a travel from the shallow platform toward a relatively distal environment. Consequently, calcirudite deposits are interpreted as the result of gravel flows or high-density turbiditiy currents coming directly from an unlithified platform. The lack of channelized features and the relative lateral continuity of the calcirudite beds suggest sheet-like deposits.

5.1.8. Medium to fine-grained calcarenite deposits (type 2-calcarenite)

Normally-graded calcarenite beds, with coarser grains at the base, basal scours, planar, oblique and convolutes laminations (Figs. 7c, d, 8a) may be interpreted as fine-grained carbonate turbidites, probably deposited by high- to low-density turbidity current (sensus Talling et al., 2012). These deposits commonly occur inside relatively thick marly intervals containing thin siderite layers, showing the distal feature of these deposits.

5.2. Depositional model

Interpretations of redeposited carbonate systems mainly rely on the study of the lateral relationship between the carbonate platform and the distal areas where redeposited carbonates deposited. However, for the Bakio Breccias Formation, the absence of the source area, which has been completely eroded and the absence of the distal areas, which are not well exposed make the interpretation difficult. Consequently, the following interpretations mainly rely on the facies observations and the vertical architecture of the Bakio Breccias Formation, from the exposures in the coastline (Figs. 3a, 4).

Sub-unit 1 is dominated by thick clast-supported breccia beds with large margin-derived limestone blocks, stacked together or interbedded with thin-bedded calcarenite beds and marly intervals (Fig. 4). Clast-supported breccia and associated calcarenite beds are interpreted as resulting from rock falls from the platform margin, followed by grain flows. Clast-supported breccia and associated calcarenite beds are assumed to be the dominant deposits in the proximal lower slope and to stack together at the toe of a steep platform margin. Sub-units 2 and 3 are dominated by thick slumps and matrix-supported breccia beds, alternating with thick marly intervals and thin beds of calcarenite, calcirudite and clast-supported breccia (Fig. 4). Slumps and matrix-supported breccia beds interpreted as high strength cohesive debris flows (sensus Talling et al., 2012) indicate frequent failures of the slope. Lenticular or channelized matrix-supported breccia and siderite-bearing clast-supported breccia beds (Figs. 9, 10b) may correspond to small canyon or gullies (e:g: Eberli et al., 2004; Janson et al., 2011). Calcirudite and medium to fine-grained calcarenite layers are assumed to result from high and low-density turbidity currents. Sub-units 2 and 3 exhibit more distal features compared to sub-unit 1, and thus develop in the lower slope. The facies association found in the Bakio Breccias Formation is similar to several Aptian-Albian carbonate slopes, in the Basque-Cantabrian basin, where the associated platform exhibits packstones or grainstones locally with orbitolinids in the shallow internal areas, rudistids and corals faunas at the platform margin, and breccia on the slope with limestone blocks deriving from the margin (García-Mondéjar and Fernández-Mendiola, 1993; Rosales, 1999; Gómez-Pérez et al., 1999; Fernández-Mendiola et al., 2013).

The carbonate platform from where the Bakio Breccias Formation was sourced is not currently observed. But several elements indicate that this platform developed on the topographic relief top of the Bakio diapir,

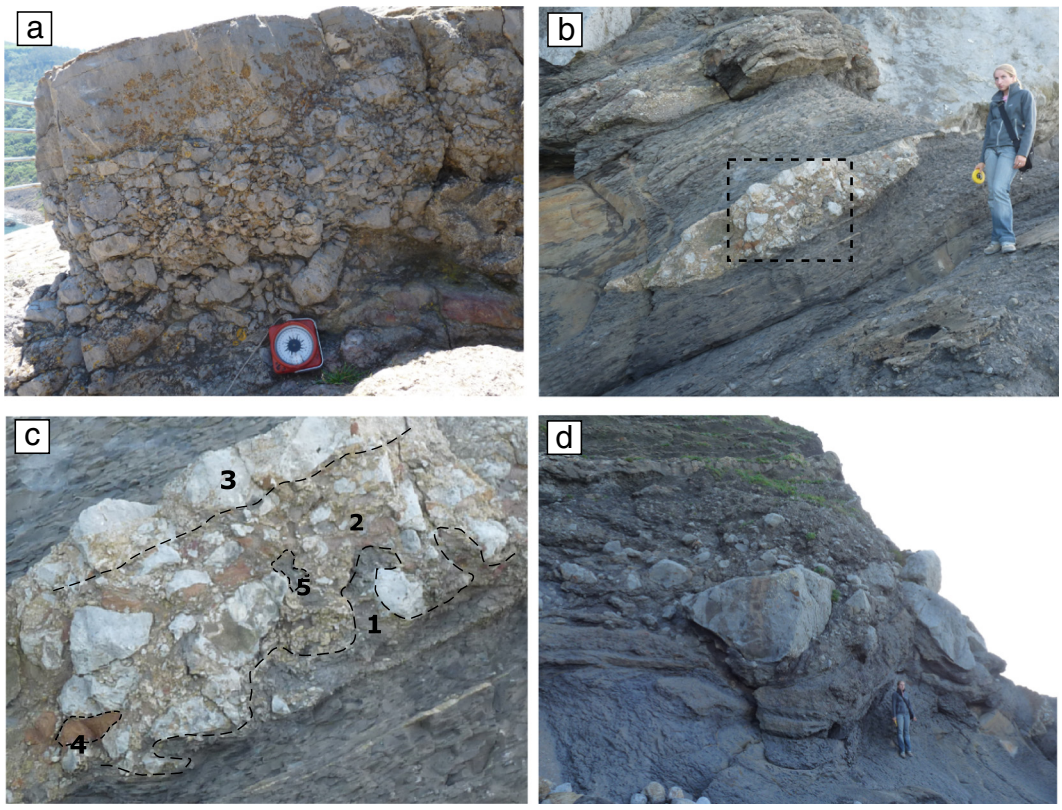

Fig. 9. Pictures of clast and matrix-supported breccia beds. a. Single bed with a normal grading from clast-supported breccia to calcarenite showing the clast-supported texture of these deposits. b. Channelized clast-supported breccia with siderite pebbles interbedded with marls. c. Details of b. showing a marly matrix at the base of the bed (1), a mixed matrix with marls, limestone blocks and gravels and siderite pebbles, in the central part of the bed (2), limestone blocks concentrated at the top of the bed (3), siderite pebble (4) and locally marly clast (5). d. Normally graded matrix-supported breccia with angular floatstone blocks within a marly matrix.

similar to other diapirs worldwide (e.g. Davison et al., 1996; Bantan, 1999; Bosence et al., 1998; Carbone et al., 1998; Orszag-Sperber et al., 1998; Giles and Lawton, 2002; Pirazzoli et al., 2004; Bosence, 2005; Jaillard et al., 2013) and in the Basque-Cantabrian basin (García-Mondéjar and Robador, 1987; Fernández-Mendiola and García-Mondéjar, 1997). First, mapping reveals that the Bakio Breccias Formation is present only around the Bakio diapir. This formation pinches out toward the diapir and thins away from the diapir (Fig. 3a). Second, Poprawski et al. (2014) using dip-angles and fold-axis directions, demonstrated that slumps with limestone blocks in both flanks of the diapir were sliding from the diapir roof (Fig. 3a). Third, breccia with blocks, locally up to 2 metres large (Figs. 8d, 9d), suggests only a short run-out distance, less than 10 km, since redeposited carbonate systems are commonly small-sized (e.g. Mullins and Cook, 1986; Spence and Tucker, 1997; Playton et al., 2010). For example, Mulder et al. (2012a) describe 3 km long gullies related to slope failure and mass transport processes in the Bahamas. All the elements above demonstrate that the breccia could only be sourced from a platform that developed on top of the topographic relief created by the Bakio diapir, as originally postulated by García-Mondéjar and Robador (1987); Robles et al. (1988).

During Albian, a regional deepening occurred, driven by subsidence of the Basque Trough (Gómez et al., 2002; García-Mondéjar et al., 2005) and by the global sea-level rise (Vail et al., 1977; Haq et al., 1987; Brunet, 1997; De Graciansky, 1998). At regional scale, this deepening induced the partial drowning of carbonate platforms and the deposition of siliciclastic turbidites (Black Flysch Group) (Fig. 2b), which are overlying the Bakio Breccias Formation (Punta de Bakio and Sollube units). Despite this regional deepening, the vertical succession from the Bakio marls unit to sub-unit 1 shows an apparent shallowing, since the Bakio marls unit is interpreted as deposited in an outer shelf setting (García-Mondéjar and Robador, 1987; Robles et al., 1988), while sub-unit 1 is interpreted as deposited at the toe of a carbonate platform margin. This apparent shallowing trend is limited only to the lower part of sub-unit 1, since the upper part displays thinning and finning upward features (Fig. 4). Since the apparent shallowing occurred independently of the regional deepening and as it was coeval with the creation of the angular unconformity at the base of sub-unit 1, it may be explained by a carbonate platform that kept up with the relative sea-level rise by aggradation favoured by the diapir rise (Fig. 11a).

The vertical succession from sub-unit 1 to sub-unit 2 (Fig. 3) with a progressive vertical increase of distal facies and the presence of orbitolinids in sub-units 2 and 3 (Fig. 7b), commonly associated with transgressive events (e.g. Rosales, 1999; Gómez-Pérez et al., 1999; Skelton and Gili, 2012) may be explain by the regional overall deepening during the Albian (Fig. 11b). Several works in carbonate (e.g. Playton and Kerans, 2002; Janson et al., 2007, 2011; Playton, 2008) show that carbonate breccias deposition are more common during the deposition of late TST and early HST due to carbonate platform aggradation and the associated collapse of the steep platform margins. Consequently, sub-units 1, 2 and 3 (Fig. 3) are interpreted to deposit during carbonate platform aggradation (Fig. 11b) which may explain the presence of breccias with blocks up to 2 m large. In such aggradating platforms, steep escarpments related to large scale collapse of the platform margin are common (e.g. Eberli et al., 1993; Borgomano, 2000; Savary and Ferry, 2004; Janson et al., 2011; Principaud et al., 2015; Jo et al., 2015; Tournadour et al., 2015; Playton and Kerans, 2015). The vertical and irregular escarpment located on the Gaztelugatxe Island (Fig. 3a), previously interpreted as a normal fault (Poprawski et al., 2014), about 1 km NE of the Bakio diapir could also be interpreted as a steep depositional escarpment with or without a structural control. The orientation of the escarpment that can be roughly extrapolated southward along the strike of the eastern flank suggests that diapir

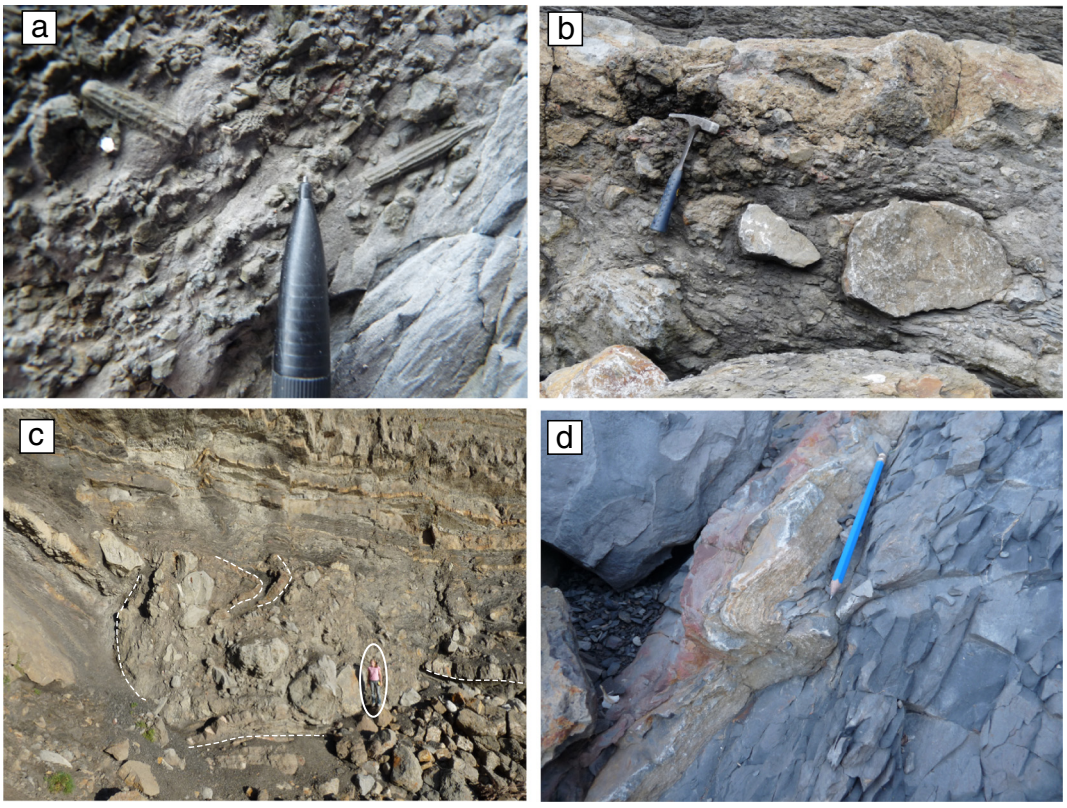

Fig. 10. Pictures of matrix-supported breccia beds and slumps. a. Details of the matrix of a matrix-supported breccia bed showing a mix between marl and limestone debris with limestone gravels and regular urchin spines. b. Inversely graded composite bed with a transitional contact between matrix-supported breccia at the base and clast-supported breccia at the top. c. Details of slumps found at the toe of the Gaztelugatxe escarpment with lateral variation from slump to matrix-supported breccia. d. Detail of a slumped, fine-grained calcarenite bed.

growth controlled the location of the platform margin (Fig. 3a). The presence of such escarpment supports the hypothesis of the aggradation of a platform on top of the diapir, creating a thick diapir roof on the northern part of the diapir. At the end of the deposition of sub-units 2 and 3, the onlap of sub-unit 2 on the Gaztelugatxe escarpment suggests the backstepping of the platform, toward the north. This suggests that the carbonate platform was connected to the Landes Massif to the north. Above the Bakio Breccias Formation, the units of the Black Flysch Group indicate the drowning of the carbonate platform top on of the Bakio diapir.

5.3. Halokinetic sequences in the Bakio Breccias Formation

Previous studies already demonstrated the effects of halokinesis on the Albian rocks around the Bakio diapir, since Rowan et al. (2012b); Poprawski et al. (2014); Ferrer et al. (2014) interpreted the growth strata and the angular unconformities (Figs. 5, 6) as a result of diapir growth. In the Punta de Bakio unit, overlying the Bakio Breccias Formation, wedge halokinetic sequences have also been described Poprawski et al. (2014). In the Bakio Breccias Formation, the presence of growth strata (Fig. 6) and angular unconformity (Fig. 5) also suggests deposition during diapir growth as described above and the formation of halokinetic sequences. However, clinoforms or differential compaction between basinal and platform facies may also create relatively high angle sedimentary dips, without significant diapir flanks rotation. For example, clinoforms may have high depositional angle from 25 up to 45° (e.g. Kenter, 1990; Cronin et al., 2000; Blendinger, 2001; Keim and Schlager, 2001; Della Porta et al., 2004) in grain- and clast-supported slopes and up to 5° in muddy slopes (e.g. Kenter, 1990). Differential compaction may lead to post-sedimentation rotation reaching an angle of 10° (Saller, 1996). Consequently, detection of halokinetic sequences using bedding dips only in carbonates is not straightforward and warrant a discussion whether these dips result of passive diapir growth, clinoforms deposition or differential compaction.

In the northern part of the eastern flank of the Bakio diapir, the first structure possibly related to diapir growth is the angular unconformity at the base of the Bakio Breccias Formation, where an angle of 40° is found between the beds of the Bakio Breccias Formation and the underlying Bakio marls unit (Fig. 5). The later unit consists of interbedded marls and thin-bedded packstones, interpreted as deposited in an outer shelf setting (García-Mondéjar and Robador, 1987; Robles et al., 1988). In such facies, the presence of clinoforms is excluded and differential compaction is unlikely since these facies are relatively distal. Consequently, the angular unconformity may be interpreted as the upper boundary of a CHS developed in the Bakio marls unit. The high angle and the overturned beds in the Bakio marls unit (Fig. 5) that parallels to the diapir contact suggests the presence of hook halokinetic sequences stacking into a tabular CHS, called CHS 1 (Fig. 12a).

The growth strata in the southern part of the eastern flank displays a total angle between the most and less dipping beds in the entire Bakio Breccias Formation reaching 45°, and several beds are overturned, near the contact with the diapir (dipping 80° NW) (Fig. 3a). In this area, the Bakio Breccias Formation is relatively muddy with thick marls intervals and matrix-supported breccias and thus may be considered as deposited in muddy slope. Assuming a maximal dip angle in muddy slopes (up to 5°) combined with differential compaction (possibly up to 10°, according to Saller, 1996), halokinetic rotation of the eastern flank of the diapir (up to 30°) is needed to explain the total angle of 45° between the most and less dipping beds. Consequently, in this area, the Bakio Breccias Formation is interpreted to form a tapered CHS, called CHS 2 (Fig. 12a). Further north, in sub-unit 1, the total angle between the most and less dipping beds reaches only 25° (Fig. 4). Sub-unit 1 is mainly clast-supported (Fig. 4), thus clinoforms

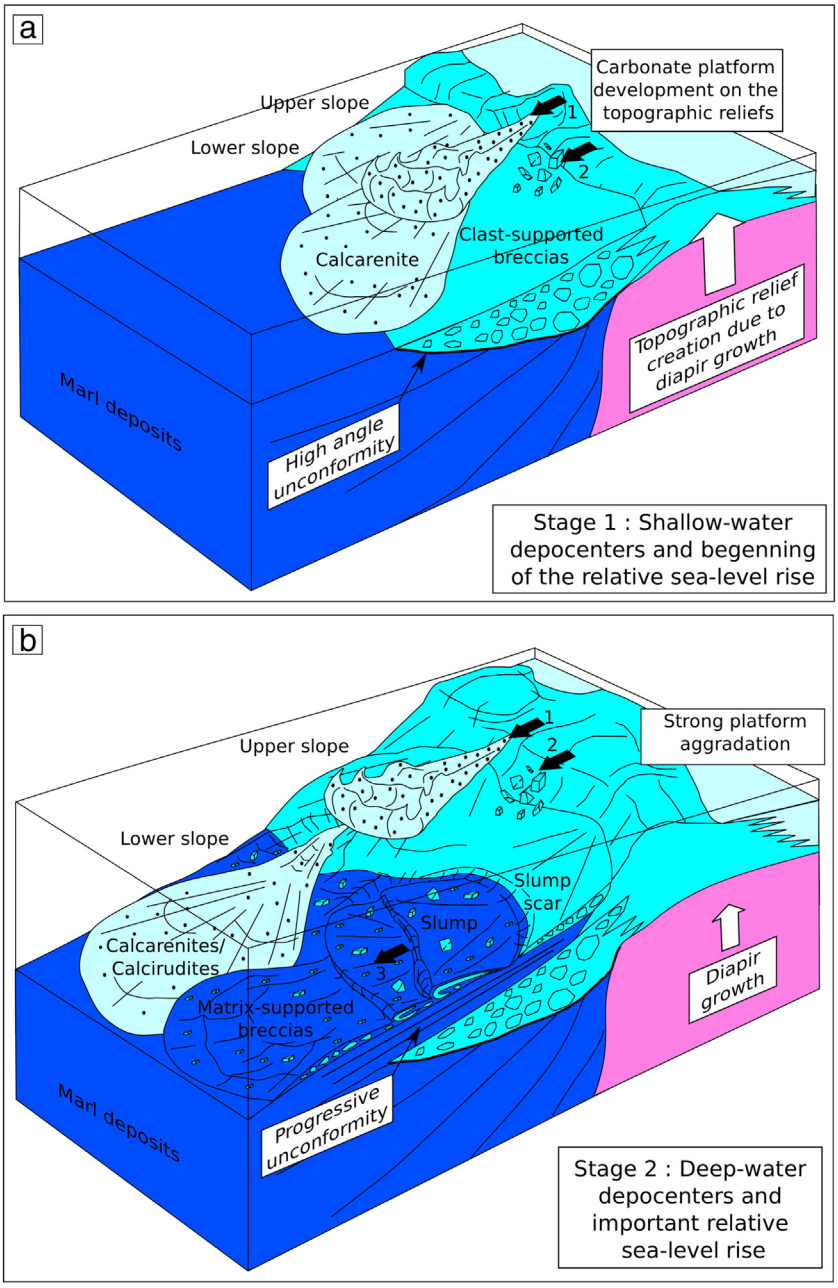

Fig. 11. Depositional model for the Bakio Breccias Formation. a. During the deposition of sub-unit 1, topographic relief created by diapir growth and coincided to the regional Albian deepening of the Basque Trough. Apparent shallowing due to relief creation allowed the creation of the carbonate platform top of the Bakio diapir. The regional Albian deepening forced the platform to aggrade rapidly after a possible rapid stage of progradation top of the Bakio marls unit. Slope destabilizations combined with early lithification processes favoured the export of a large amount of lithified limestones debris in the relatively shallow adjacent depocenters, explaining the presence of clast-supported redeposited carbonate. Black arrows 1 and 2 represent grain flow and rock fall, respectively. b. During the deposition of sub-units 2 and 3, the carbonate platform may be able to keep up with the relative sea-level rise, leading to vertical aggradation of the platform, on top of the diapir. The adjacent depocenters became relatively deeper, which explain the mix between limestones debris together with distal facies forming matrix-supported redeposited carbonate. Black arrows 1, 2 and 3 represent grain flow, rock fall and high strength cohesive debris flow, respectively.

in this unit may reach an angle up to 45° (e.g. Kenter, 1990; Cronin et al., 2000; Blendinger, 2001; Keim and Schlager, 2001; Della Porta et al., 2004). Consequently, it is not possible to decipher whether the variations of bedding dips in sub-unit 1 are related to initial slope geometries or to slight diapir flank rotation. However, the growth strata found in sub-unit 1 (Fig. 4) may be laterally correlated along the strike of the eastern flank with the tapered CHS 2, defined further south (Fig. 3a), since they are time-equivalent, suggesting that the northern part of the eastern diapir flank was also affected by rotation. Different angles of rotation along strike in the same CHS suggest lateral variations in diapir growth. In the southern part of CHS 2, the total angle of rotation is up to 30° for the entire Bakio Breccias Formation, while it is less than 25° in sub-unit 1 in the northern part. It suggests a faster diapir growth velocity in the southern part of the diapir, as already postulated by Poprawski et al. (2014). Such difference between the north and the south may be explained by the initial geometry of the carbonate platform, which is interpreted to be thicker north of the diapir, forming a resistant roof that limited diapir growth. This geometry of the platform is supported by the presence of relatively proximal facies (Sub-unit 1) occurring only in the northern part of the diapir and of marly facies occurring

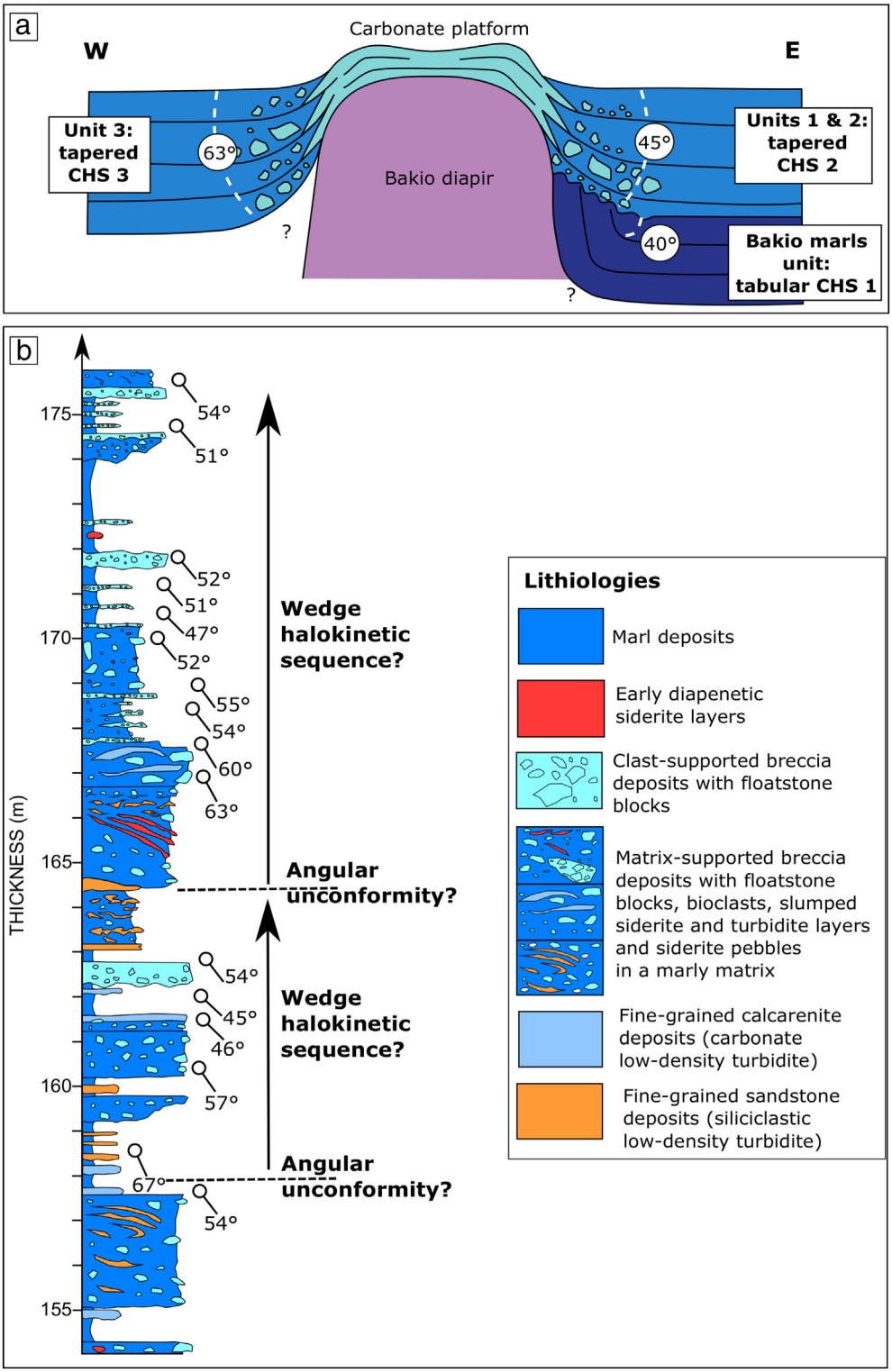

Fig. 12. a. Interpretation of the carbonate-dominated CHS from the Bakio diapir flanks. CHS 1 coincides with the Bakio marls unit, CHS 2 with sub-units 1 and 2 and CHS 3 with sub-unit 3. Wedge halokinetic sequences described in the Punta de Bakio unit (see the bedding dips variations in Fig. 4) by Poprawski et al. (2014) also belong to the upper part of the CHS 3. b. Detailed stratigraphic section in CHS 3, in the western flank of the Bakio diapir (location Fig. 4). The upward decrease of the bedding dips is not homogeneous and may be interpreted as related to the presence of wedge halokinetic sequences. Breccia deposits do not display any apparent organisation in the vertical facies succession, suggesting that several combined processes as diapir flank rotation, carbonate production and early lithification control the slope stability. The absence of vertical organisation in breccia deposits makes difficult the recognition of halokinetic sequences in carbonate settings.

only in the southernmost part of the diapir (Fig. 11a). Giles and Rowan (2012) highlighted that tapered CHS above tabular CHS commonly produce important drape folding and overturned strata due to a superimposed broad area of folding on the overlying tabular CHS. According to this interpretation, the vertical succession from the Bakio marls unit to sub-unit 1, forming a tapered CHS and a tabular CHS (Fig. 12a), respectively, is assumed to explain the presence of overturned beds in the Bakio marls unit (Fig. 4).

In the growth strata west of Bakio (Fig. 6), the total angle between the most and less dipping beds reaches 63° in the Bakio Breccias Formation (sub-unit 3) and several beds are overturned, near the contact with the diapir (dipping 80° SE). Sub-unit 3 is relatively muddy with thick marls intervals and matrix-supported breccias (Fig. 4) and may be considered as deposited in muddy slope. Assuming a maximal dip angle in muddy slopes (up to 5°) and differential compaction (possibly up to 10°, according to Saller, 1996), halokinetic rotation of the western flank of the diapir (up to 48°) is needed to explain the total angle of 63° between the most and less dipping beds in sub-unit 3. Consequently, sub-unit 3 is interpreted to form a tapered CHS, called CHS 3 (Fig. 12a), as already described by since Rowan et al. (2012b); Ferrer et al. (2014) with a broad area of drape folding, up to 350 m away from the diapir. In details, sub-unit 3 shows sedimentary packages, about 10 m thick, with an upward decreasing bedding dips (Fig. 12b) that may be interpreted as wedge halokinetic sequences, stacked into the CHS 3. The absence of organisation in the vertical facies succession in these wedge halokinetic sequences, with erratic occurrence of breccia layers (Fig. 12b) suggests that the slope stability was mainly controlled by carbonate platform growth rather than by diapir growth. Since sub-units 2 and 3 are probably time equivalent, the upper part of tapered CHS 2 and the tapered CHS 3 probably formed at the same time.

6. Discussion: halokinetic sequences in carbonate systems

This is not clearly mentioned in literature, but the halokinetic sequence models (Giles and Lawton, 2002; Rowan et al., 2003; Giles and Rowan, 2012) refer to siliciclastic sediments, since only an external sedimentary input, filling the mini-basins and progressively onlapping the diapir flanks is inferred (Fig. 1). There is a major limitation with this model when applied to carbonates, since they do not result from an external sedimentary input, rather from local carbonate production. Moreover, carbonate platforms are able to keep up with relative sea-level rise by aggradation that may favour the creation of steep slopes (e.g., Kendall and Schlager, 1981; Pomar, 2001; Bosence, 2005; Pomar and Hallock, 2008). The presence of reef-building species (e.g., Pomar, 2001; Bosence, 2005; Pomar and Hallock, 2008) combined with early lithification occurring during sedimentation (Moore, 1989; Flügel, 2004; Tucker and Wright, 2009) may also favour the early cementation of the diapir roof. Additionally, karstification can occur if the diapir roof is emerged. Such processes do not exist in siliciclastic sedimentation, suggesting that carbonate-dominated halokinetic sequences should differ from their siliciclastic counterparts.

The carbonate Composite Halokinetic Sequences, found in the Bakio diapir flanks (Fig. 12a) illustrate several differences compared to the siliciclastic CHS. In siliciclastic tapered CHS, gravity-driven deposits are assumed to be rare (Fig. 1g) since sediments onlapping on the diapir flanks create relatively stable slopes (Giles and Lawton, 2002; Rowan et al., 2003; Giles and Rowan, 2012). In contrast, the tapered CHS 2 and 3 from Bakio displays blocks up to 2 m large (Fig. 4), suggesting the collapse of a steep margin, coming from the Gaztelugatxe escarpment in the eastern flank. Such difference results from the ability of the carbonate platform to aggrade, creating steep slopes and leading to the partial collapse of the margin, even if only limited relief was created by diapir growth. The absence of organisation in the vertical facies succession in CHS 2 and 3, with erratic occurrence of breccia layers (Fig. 12b) also suggests that the slope stability was mainly controlled by carbonate platform growth rather than by just diapir growth. Therefore, gravity-driven deposits with platform-derived clast are probably more common in carbonate-dominated CHS, even in tapered CHS compared their siliciclastic counterparts. According to several recent works in carbonate settings, carbonate breccias deposition mainly occur during the deposition of late TST and early HST when the carbonate platforms are the most likely to aggrade and create steep platform margins that may overstep and collapse. In contrast, during late HST, carbonate platform margins are more likely to have grainy shoals development associated with margins progradation and limited accommodation space that will result in more grain-dominated gravity flow deposit in the adjacent slope and basin (e.g., Playton and Kerans, 2002; Janson et al., 2007, 2011; Playton, 2008). This suggests that carbonate-dominated CHS developed during TST may display gravity-driven deposits with clast-derived from the platform, while CHS developed during late HST may be mainly grain-supported (Fig. 13).

In the literature, the halokinetic sequences are commonly linked to regional sea-level variations and correlated with depositional sequences and system tracts. In the Bakio area, system tracts cannot be definitely recognized because of absence of the shallow-water facies and dominance of relatively deep-water facies. Nonetheless using other studies of carbonate gravity-flows (e.g. Playton and Kerans, 2002, 2015; Janson et al., 2007, 2011; Playton, 2008) as analogues and the regional evolution during the Albian, the following interpretation can be proposed: the high proportion of breccia interpreted as margin collapse, associated with the Bakio Breccias Formation facies evolution indicates backstepping patterns and the deposition during the subsidence of the Basque Trough (Gómez et al., 2002; García-Mondéjar et al., 2005) combined with global sea-level rise during Albian (Vail et al., 1977; Haq et al., 1987; Brunet, 1997; De Graciansky, 1998). These elements lead to the interpretation of a system developing during a 3rd order TST. Consequently, the CHS found in the Bakio Breccias Formation may be considered as examples of carbonate-dominated halokinetic sequences developed during a TST. In siliciclastic settings, during TST, tabular CHS commonly develop, because of low sediment accumulation (Giles and Rowan, 2012). In contrast, CHS 2 and 3 are assumed to be tapered because the carbonate platform top of the Bakio diapir was able to keep up with the sea level rise, and thus the carbonate platform was aggradating top of the diapir, forming a thick and resistant roof due to early lithification (Moore, 1989; Flügel, 2004; Tucker and Wright, 2009). Such thick and resistant roof is assumed to limit the diapir growth and thus to favour the development of tapered CHS (Fig. 13a). The influence of thick carbonate roof is also illustrated by the different angles of rotation along strike in the CHS 2, suggesting lateral variations in diapir growth, with limited diapir growth where the carbonate platform was thicker.

In the La Popa basin, in Mexico, carbonate platforms are also assumed to develop on top of diapirs during TST, but most of the associated CHS are tabular (Giles and Rowan, 2012). However, these CHS are mixed and the siliciclastic input may have limited the carbonate platform growth, therefore these CHS may not be typical of carbonate-dominated CHS. The only exception in the La Popa basin is the tapered CHS described by Giles and Rowan (2012) in the Upper mudstone Member, in the flanks of the La Popa salt wall. This tapered carbonate-dominated CHS developed in a TST and is characterized by 100 m thick and 4 km long clinoform showing an important carbonate production (Giles and Rowan, 2012). In this case, this CHS may be considered as typical for carbonate-dominated CHS that clearly shows the same trend compared to the Bakio carbonate-dominated CHS, and supports the hypothesis that carbonate-dominated CHS are preferentially tapered during TST (Fig. 13a), which differs from the siliciclastic CHS.

In the Bakio Breccias Formation, there is no example of carbonate-dominated halokinetic sequences developed during HST. Theoretically, during late HST deposition (and LST if present), the absence of accommodation space top of the diapir may lead to carbonate platform progradation in the adjacent depocenters. The ability of the diapir to reach the surface during late HST depends on the thickness of the residual roof developed during the underlying TST and to the amplitude of the sea level fall, at the end of the HST. In the case of a thick residual roof combined with low amplitude sea level fall, the roof may be preserved and may limit the diapr growth. In this case, carbonate-dominated CHS deposited tend to be tapered as during the TST (Fig. 13b). In the Central Flinders Ranges in Australia, Kernen et al. (2012) described a carbonate tapered CHS in the Green mudstone Member, in the Wonoka Formation, that developed at the end of a

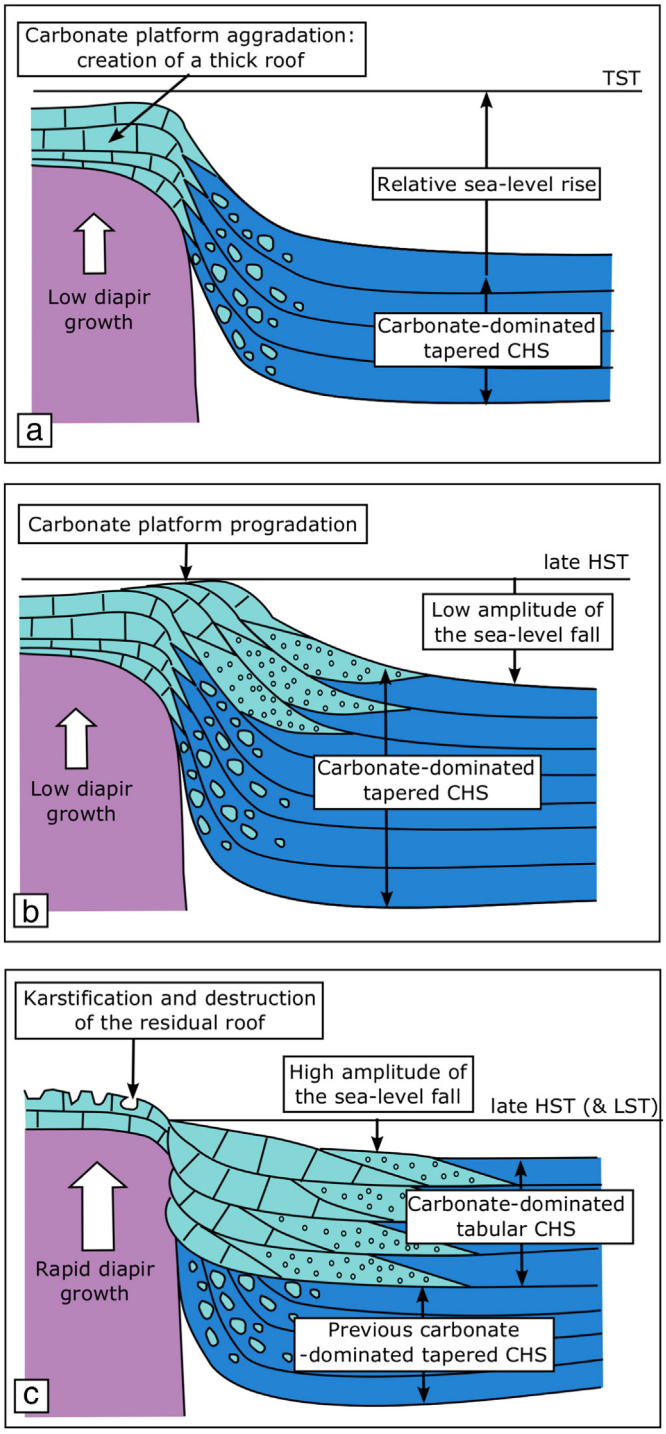

Fig. 13. Model carbonate-dominated CHS. a. During TST deposition, the carbonate-dominated CHS are assumed to be tapered because the carbonate platform top of the diapir is able to keep up with the sea level rise, forming a thick and resistant roof by aggradation. Strong sediment accumulation rate top of the diapir may limit the diapir growth velocity. b. During late HST deposition, if the residual roof formed during the previous TST is thick and if the amplitude sea level fall at the end of the HST is limited, the roof may be preserved and may limit the diapir growth. In this case, carbonate-dominated CHS deposited tend to be also tapered as during the TST. c. During late HST deposition, if the residual roof formed during the previous TST is thin and if the amplitude sea level fall at the end of the HST is important, the diapir roof is emerged and karstification favour the residual roof destruction. Consequently, significant diapir growth velocity and flank rotation occur leading to the residual roof destruction and thus carbonate-dominated CHS deposited tend to be tabular.

HST, near the sequence boundary. In this tapered CHS, they identified several clasts coming from the underlying units and interpreted to be derived from the residual diapir roof. Since the CHS is tapered, it suggests that the roof was partially preserved and thus it illustrates the case of a thick residual roof combined with low amplitude sea level fall, leading the creation of tapered CHS deposited during a late HST (Fig. 13b). In the case of a thin residual roof combined with high amplitude sea level fall at the end of the HST (Fig. 13c), carbonate platform progradation and sediment accumulation increase in the adjacent depocenters lead to the loading the autochthonous salt layer. In addition, if the diapir roof reaches emersion, karstification may also favour the residual roof destruction and thus further promote significant diapir growth and creation of topographic relief. Consequently, diapir growth velocity and flank rotation during late HST is assumed to be more important than during the TST leading to the residual roof destruction and thus carbonate-dominated CHS tends to be tabular (Fig. 13c). In the High Atlas, in Morocco, Vergés et al. (2013) describe a high angle unconformity between two relatively tabular packages of carbonate, along the Tazoult salt ridge. High angle unconformity and relatively tabular packages allow the identification of a tabular CHS. The high angle unconformity is highly karstified and may be interpreted as a sequence boundary developed top to a HST. Consequently, this example illustrates the case of a relatively thin roof combined with high amplitude sea level fall at the end of the HST, associated with a tabular CHS deposited during a late HST (Fig. 13c).

In siliciclastic settings, the basal boundary of tabular CHS commonly occurs in the early TST and the basal boundary of tapered CHS commonly occurs with the maximum flooding surface or the early HST interval. The data from the Bakio region and the other examples discussed above suggests that the basal boundary of carbonate-dominated tapered CHS may be found preferentially in the early TST (Fig. 13a) and the basal boundary of tabular CHS, when present, should preferentially occur near the maximum flooding surface or in the early HST (Fig. 13c). However, in the case of a thick roof or a limited relative sea level fall at the end of HST, CHS may be also tapered in late HST (Fig. 13b). This confirms the hypothesis developed by Giles and Rowan (2012) when they assume that carbonate-dominated CHS tend to be preferentially tapered, due to the creation of thick diapir roof by carbonate platform growth. The results of this paper are also comparable to those proposed by Hearon et al. (2014b) in deep-water setting, since they argue that the most important process controlling the geometries of the CHS is the thickness of the diapir roof. In deep-water setting, the thickness of the roof is controlled by the ratio between sediment accumulation rate and diapir growth velocity but also by slumping processes and deep-water currents that favour the destruction of the roof. In carbonate, the main factors controlling the thickness of the roof are also the ratio between sediment accumulation rate and diapir growth velocity but sea-level variations that control the depth of the photic zone and the carbonate sedimentation (Pomar, 2001) are also a key factor, since platform aggradation during TST favour the creation of a thick roof while karstification at the end of the HST favour the destruction of the roof.

Several studies describe the presence of diapir-derived clasts in the gravity-driven deposits at the base of the halokinetic sequences, showing that diapirs periodically pierce the diapir roof (Giles and Lawton, 2002; Rowan et al., 2003, 2012a; Andrie et al., 2012; Giles and Rowan, 2012; Banham and Mountney, 2013a, 2013b, 2014; Hearon et al., 2015). In the overburden of the Bakio diapir, diapir-derived clasts are absent suggesting that the diapir did not ever reach the surface during the deposition of the Bakio Breccias Formation. This supports the hypothesis of a thick and resistant roof, made of carbonate platform facies developed top of the diapir (Fig. 11). Consequently, since the carbonate-dominated CHS tend to be preferentially tapered (Fig. 12a), due to the creation of thick diapir roof, it may prevent the diapir to reach the surface and thus diapir-derived clasts are probably rarer in carbonate-dominated CHS compared to siliciclastic CHS.

7. Conclusions

The Bakio Breccias Formation provides a new outcrop-based example of carbonate-dominated halokinetic sequences associated with a carbonate platform that developed on top of a growing diapir. This study highlights new key elements concerning: (i) the local understanding of the Bakio Breccias Formation and its relationship with the Bakio diapir growth, (ii) the relationship between relative sea-level variations and carbonate CHS, and (iii) the importance of diapir flank topography and carbonate production that control the slope stability in diapir flanks. These new elements are listed below:

(i) The Bakio Breccias Formation deposited during the Albian regional deepening, driven by subsidence of the Basque Trough and by the global sea-level rise. However, the relatively shallow lower part of the Bakio Breccias Formation may be explained by creation of topographic relief, top of the Bakio diapir. Once the diapir-related topographic relief was initiated, the carbonate platform developed mainly by aggradation in response to the regional deepening, as showed by progressive vertical increase of distal facies. The first unit (sub-unit 1) is clast-dominated and is interpreted to deposit in the proximal lower slope, at the toe of the platform margin located at the edge of the diapir. The younger sub-units (sub-units 2 and 3) are mud-dominated and exhibit more distal features compared to sub-unit 1, and are assumed to develop in the lower slope, following the regional deepening trend. Carbonate platform aggradation led to the creation of steep platform margins at the edge of the diapir, associated with frequent partial failure of the slope, as showed by blocks up to 2 m large. Aggradation top of the diapir led to the creation of a thick and resistant carbonate roof top of the diapir that explains the presence of tapered CHS. After the deposition the Bakio Breccias Formation, the units of the Black Flysch Group show the drowning of the carbonate platform top of the Bakio diapir.

(ii) Carbonate-dominated halokinetic sequences are assumed to differ from their siliciclastic counterpart because carbonate deposition do not result from an external sedimentary input, but from local carbonate production, commonly taking place on paleo-highs. During TST deposition, the carbonate platform may be able to keep up with the relative sea-level rise by aggradation, creating a thick and resistant diapir roof. Consequently, diapir growth and flank rotation may be relatively limited, which may favour the development of wedge halokinetic sequences and tapered CHS. During late HST deposition (and LST if present), progradation of the carbonate platform in the adjacent depocenters may increase the load of the autochthonous salt layer. Moreover, if the diapir roof reaches emersion, karstification may also favour roof destruction, promoting significant diapir growth and creation of topographic relief. Consequently, diapir growth velocity and flank rotation is assumed to be more important during late HST compared to the TST. In the case of a thin roof combined with high amplitude sea level fall, the roof may be completely destroyed and thus associated carbonate-dominated CHS may tend to be tabular. In the case of a thick roof combined with low amplitude sea level fall, the roof may be preserved and may limit the diapir growth. In this case, carbonate-dominated CHS deposited may tend to be tapered as during the TST.

(iii) In carbonate systems, the occurrence of gravity-driven deposits may be controlled by a combination of diapir topography and carbonate production. Carbonate breccias deposition mainly occurs during the deposition of late TST and early HST due to carbonate platform aggradation associated with the collapse of the steep platform margins, while during late HST, carbonate platform margins are usually composed of grain-supported facies. This suggests that carbonate-dominated CHS developed during TST may display gravity-driven deposits, while CHS developed during late HST may be mainly grain-supported. During TST, the clasts in the CHS are assumed to be derived from the platform margin, since during TST a thick diapir roof is inferred. During late HST, in the case of a relatively high amplitude sea level fall associated with karstification, the roof may be partially or completely destroyed. In this case, clast derived from older units or from the diapir body may be found. Slope destabilization is interpreted to occur during both HST and TST in carbonate environments, which is not the case in siliciclastic environments. Consequently, carbonate-dominated halokinetic sequences are probably more difficult to recognize than their siliciclastic counterpart, because of the erratic occurrence of gravity-driven deposits, as illustrated by the Bakio Breccias Formation.

Acknowledgements

The authors would like to thank the ARNT-CIFRE and Geolink (382/2008), for the funding of the Ph.D. work of Y. Poprawski. We gratefully acknowledge Xavier Janson and Thomas Hearon for their interesting critics and comments that greatly improved the manuscript. Yohann Poprawski also would like to acknowledge the GDL Group from the ICTJA in Barcelona for the interesting discussions and comparison with other diapirs in the High Atlas.

References

Ábalos, B., Elorza, J., 2012. Structural diagenesis of siderite layers in black shales (Albian black flysch, Northern Spain). Journal of Geology 120, 405–429.
Ábalos, B., Alkorta, A., Iríbar, V., 2008. Geological and isotopic constraints on the structure of the Bilbao anticlinorium (Basque–Cantabrian basin, North Spain). Journal of Structural Geology 30, 1354–1367.
Agirrezabala, L., 1996. El Aptiense-Albiense del Anticlinorio Nor-Vizcaino entre Gernika y Azpeitia Ph.D. thesis Euskal Herriko Unibertsitatea, Bilbao, Spain.
Alves, T.M., Manuppella, G., Gawthorpe, R.L., Hunt, D.W., Monteiro, J.H., 2003. The depositional evolution of diapir- and fault-bounded rift basins: examples from the Lusitanian Basin of West Iberia. Sedimentary Geology 162, 273–303.
Andrie, J.R., Giles, K.A., Lawton, T.F., Rowan, M.G., 2012. Halokinetic-Sequence Stratigraphy, Fluvial Sedimentology and Structural Geometry of the Eocene Carroza Formation along La Popa Salt Weld, La Popa Basin, Mexico. In: Archer, S.G., Alsop, G.I., Hartley, A.J., Grant, N.T., Hodgkinson, R. (Eds.), Salt Tectonics, Sediments and Prospectivity vol. 363. Geological Society of London, Special Publications, pp. 59–79.
Arbués, P., Ferrrer, O., Roca, E., Giles, K., Rowan, M., De Matteis, M., Muñoz, J.A., 2012. The Bakio Salt Wall and its Effects on Synkinematic Deepwater Sedimentation (Basque Pyrenees, Northern Spain). EGU General Assembly Conference Abstracts, Vol. 14, Vienna, Austria, p. 9659.
Badillo, J.M., García-Mondéjar, J., Pujalte, V., 1983. Análisis del Flysch Negro (Albiense Superior-Cenomaniense Inferior) en la Bahía de Arminza. Comunicaciones del X Congreso Nacional de Sedimentología, Grupo Español de Sedimentología, Pomar, L., Palma de Mallorca, Spain, pp. 4.6–4.9.
Bahamonde, J.R., Kenter, J.A., Della Porta, G., Keim, L., Immenhauser, A., Reijmer, J.J., 2004. Lithofacies and depositional processes on a high, steep-margined Carboniferous (Bashkirian–Moscovian) carbonate platform slope, Sierra del Cuera, NW Spain. Sedimentary Geology 166, 145–156.
Banham, S.G., Mountney, N.P., 2013a. Controls on fluvial sedimentary architecture and sediment-fill state in salt-walled mini-basins: Triassic Moenkopi Formation, Salt Anticline Region, SE Utah, USA. Basin Research 25, 709–737.
Banham, S.G., Mountney, N.P., 2013b. Evolution of fluvial systems in salt-walled mini-basins: A review and new insights. Sedimentary Geology 296, 142–166.
Banham, S.G., Mountney, N.P., 2014. Climatic versus halokinetic control on sedimentation in a dryland fluvial succession. Sedimentology 61, 570–608.
Bantan, R., 1999. Geology and sedimentary environments of Farasan Bank (Saudi Arabia), southern Red Sea: a combined remote sensing and field study Ph.D. thesis London University, London, UK.
Blendinger, W., 2001. Triassic carbonate buildup flanks in the Dolomites, Northern Italy: breccias, boulder fabric and the importance of early diagenesis. Sedimentology 48, 919–933.
Borgomano, J.R.F., 2000. The Upper Cretaceous carbonates of the Gargano-Murge region, Southern Italy: a model of platform-to-basin transition. American Association of Petroleum Geologists Bulletin 84, 1561–1588.
Bosence, D., 2005. A genetic classification of carbonate platforms based on their basinal and tectonic settings in the Cenozoic. Sedimentary Geology 175, 49–72.
Bosence, D., Al-Aawah, M., Davison, I., Rosen, B., Vita-Finzi, C., Whitaker, E., 1998. Salt domes and their control on basin margin sedimentation: a case study from the

Tihama Plain, Yemen. In: Purser, B.H., Bosence, D. (Eds.), Sedimentation and Tectonics in Rift Basins Red Sea:-Gulf of Aden. Springer, Netherlands, pp. 448–454.
Bouma, A.H., 1962. Sedimentology of some Flysch Deposits: A Graphic Approach to Facies Interpretation. Elsevier (168 pp).
Brunet, M., 1997. Subsidence along the ECORS Bay of Biscay. Mémoires. Société Géologique de France 171, 167–176.
Callot, J.-P., Ribes, C., Kergaravat, C., Bonnel, C., Temiz, H., Poisson, A., Vrielynck, B., Salel, J.-F., Ringenbach, J.-C., 2014. Salt tectonics in the Sivas basin (Turkey): crossing salt walls and minibasins. Bulletin de la Societe Geologique de France 185, 33–42.
Carbone, F., Matteucci, R., Angelucci, A., 1998. Present-day sedimentation on the carbonate platform of the Dahlak Islands, Eritrea. In: Purser, B.H., Bosence, D. (Eds.), Sedimentation and Tectonics in Rift Basins Red Sea:-Gulf of Aden. Springer, Netherlands, pp. 523–536.
Castañares, L.M., Robles, S., Gimeno, D., Vicente Bravo, J.C., 2001. The Submarine Volcanic System of the Errigoiti Formation (Albian-Santonian of the Basque-Cantabrian Basin, Northern Spain): Stratigraphic Framework, Facies, and Sequences. Journal of Sedimentary Research 71, 318–333.
Chaler, R., Dorronsoro, C., Grimalt, J., Agirrezabala, L., Fernández-Mendiola, P., García-Mondejar, J., Gómez-Pérez, I., López-Horgue, M., 2005. Distributions of C22–C30 even-carbon-number n-alkanes in ocean anoxic event 1 samples from the Basque-Cantabrian Basin. Naturwissenschaften 92, 221–225.
Cronin, B.T., Gürbüz, K., Hurst, A., Satur, N., 2000. Vertical and lateral organization of a carbonate deep-water slope marginal to a submarine fan system, Miocene, Southern Turkey. Sedimentology 47, 801–824.
Davison, I., Bosence, D., Alsop, G.I., Al-Aawah, M.H., 1996. Deformation and Sedimentation around Active Miocene Salt Diapirs on the Tihama Plain, northwest Yemen. In: Alsop, G.I., Blundell, D.J., Davison, I. (Eds.), Salt Tectonics vol. 100. Geological Society of London, Special Publications, pp. 23–39.
De Graciansky, P.C., 1998. Mesozoic and Cenozoic Sequence Stratigraphy of European Basins: Maps. 60. Sociey for Sedimentary Geology.
Della Porta, G., Kenter, J.A.M., Bahamonde, J.R., 2004. Depositional facies and stratal geometry of an Upper Carboniferous prograding and aggrading high-relief carbonate platform (Cantabrian Mountains, N Spain). Sedimentology 51, 267–295.
Drzewiecki, P.A., Simó, J., 2002. Depositional processes, triggering mechanisms and sediment composition of carbonate gravity flow deposits: examples from the Late Cretaceous of the south-central Pyrenees, Spain. Sedimentary Geology 146, 155–189.
Eberli, G.P., Bernoulli, D., Sanders, D., Vecsei, A., 1993. From Aggradation to Progradation: The Maiella Platform, Abruzzi, Italy. In: Simó, T., Scott, R.W., Masse, J.P. (Eds.), Cretaceous Carbonate Platforms vol. 56. American Association of Petroleum Geologists Memoir, pp. 213–232.
Eberli, G.P., Anselmetti, F.S., Betzler, C., Van Konijnenburg, J.H., Bernoulli, D., 2004. Carbonate platform to basin transitions on seismic data and in outcrops: Great Bahama Bank and the Maiella platform margin, Italy. In: Eberli, G.P., Masaferro, J.L., Rick Sarg, J.F. (Eds.), Seismic imaging of carbonate reservoirs and systems vol. 81. American Association of Petroleum Geologists Memoir, pp. 207–250.
Emmerich, A., Zamparelli, V., Bechstädt, T., Zühlke, R., 2005. The reefal margin and slope of a Middle Triassic carbonate platform: the Latemar (Dolomites, Italy). Facies 50, 573–614.
Fernández-Mendiola, P.A., García-Mondéjar, J., 1997. Isolated carbonate platform of Caniego, Spain: A test of the latest Albian worldwide sea-level changes. Geological Society of America Bulletin 109, 176–194.
Fernández-Mendiola, P., Mendicoa, J., Hernandez, S., Owen, H., García-Mondéjar, J., 2013. A facies model for an Early Aptian carbonate platform (Zamaia, Spain). Facies 59, 529–558.
Ferrer, O., Roca, E., Benjumea, B., Muñoz, J., Ellouz, N., MARCONI-Team, 2008. The deep seismic reflection MARCONI-3 profile: role of extensional Mesozoic structure during the Pyrenean contractional deformation at the eastern part of the Bay of Biscay. Marine and Petroleum Geology 25, 714–730.
Ferrer, O., Arbués, P., Roca, E., Giles, K., Rowan, M.G., De Matteis, M., Muñoz, J.A., 2014. Effect of Diapir Growth on Synkinematic Deepwater Sedimentation: The Bakio Diapir (Basque-Cantabrian Basin, Northern Spain). American Association of Petroleum Geologists Annual Convention and Exhibition, Houston, USA.
Flügel, E., 2004. Microfacies of Carbonate Rocks: Analysis, Interpretation and Application. Springer, Berlin.
Franseen, E.K., Goldstein, R.H., Farr, M.R., 1998. Quantitative controls on location and architecture of carbonate depositional sequences: Upper Miocene, Cabo de Gata region, SE Spain. Journal of Sedimentary Research 68, 283–298.
García-Mondéjar, J., Fernández-Mendiola, P.A., 1993. Sequence stratigraphy and systems tracts of a mixed carbonate and siliciclastic platform-basin setting: the Albian of Lunada and Soba, Northern Spain. American Association of Petroleum Geologists Bulletin 77, 245–275.
García-Mondéjar, J., Robador, A., 1987. Sedimentación y paleografía del complejo urgoniano (Aptiense-Albiense) en el área de Bermeo (región Vasco-Cantábrica septentional). Acta Geologica Hispánica 21, 411–418.
García-Mondéjar, J., Agirrezabala, L.M., Aranburu, A., Fernández-Mendiola, P.A., Gómez-Pérez, I., López-Horgue, M., Rosales, I., 1996. Aptian— Albian tectonic pattern of the Basque— Cantabrian Basin (Northern Spain). Geological Journal 31, 13–45.
García-Mondéjar, J., Fernández-Mendiola, P., Agirrezabala, L., Aranburu, A., López-Horgue, M., Iriarte, E., Martinez de Rituerto, S., 2004. Extensión del Aptiense-Albiense en la Cuenca Vasco-Cantábrica. Geología de España, Sociedad Geológica de España-Instituto Geológico y Minero de España, Madrid, pp. 340–343.
García-Mondéjar, J., López-Horgue, M.A., Aranburu, A., Fernández-Mendiola, P.A., 2005. Pulsating subsidence during a rift episode: stratigraphic and tectonic consequences (Aptian–Albian, Northern Spain). Terra Nova 17, 517–525.
Garrote, A., García Portero, J., Muñoz-Jimenez, L., Arias, V., Apalategui, O., Eguiguren, E., García Pascual, I., Zapata, M., Sánchez Carretero, R., Garrote, R., Hidalgo, J., del Val, J., 1995. Mapa Geológico del País Vasco a escala 1:100.000 y memoria. Departamento de industria, Agricultura y Pesca del Gobierno Vasco, pp. 1–345.
Giles, K.A., Goldhammer, R.K., 2000. Patterns of Reef Accretion Associated with Salt Diapirism, La Popa Basin, Mexico. American Association of Petroleum Geologists Annual Convention, New Orleans, USA.
Giles, K.A., Lawton, T.F., 2002. Halokinetic sequence stratigraphy adjacent to the El Papalote diapir, Northeastern Mexico. American Association of Petroleum Geologists Bulletin 86, 823–840.
Giles, K.A., Rowan, M.G., 2012. Concepts in Halokinetic-Sequence Deformation and Stratigraphy. In: Archer, S.G., Alsop, G.I., Hartley, A.J., Grant, N.T., Hodgkinson, R. (Eds.), Salt Tectonics, Sediments and Prospectivity vol. 363. Geological Society of London, Special Publications, pp. 7–31.
Giles, K.A., Druke, D.C., Mercer, D.W., Hunnikut-Mack, L.E.L.A., 2008. Controls on Upper Cretaceous (Maastrichtian) heterozoan carbonate platforms developed on salt diapirs, La Popa Basin, NE Mexico. In: Lukasik, J., Simo, J.A. (Eds.), Controls on carbonate platform and reef development vol. 89. Special Publication, Society for Sedimentary Geology (SEPM), pp. 107–124.
Goldstein, R.H., Franseen, E.K., Dvoretsky, R.A., Sweeney, R.J., 2012. Controls on focused-flow and dispersed-flow depwater carbonates: Miocene Agua Amarga basin, Spain. Journal of Sedimentary Research 82, 499–520.
Gómez, M., Vergés, J., Riaza, C., 2002. Inversion tectonics of the northern margin of the Basque Cantabrian Basin. Bulletin de la Societe Geologique de France 173, 449–459.
Gómez-Pérez, I., Fernández-Mendiola, P.A., García-Mondéjar, J., 1999. Depositional architecture of a rimmed carbonate platform (Albian, Gorbea, western Pyrenees). Sedimentology 46, 337–356.
Grammer, G.M., Ginsburg, R.N., Harris, P.M., 1993. Timing of Deposition, Diagenesis, and Failure of Steep Carbonate Slopes in Response to a High-Amplitude/High-Frequency Fluctuation in Sea Level, Tongue of the Ocean, Bahamas Chapter 4 In: Loucks, R.G., Sarg, J.F. (Eds.), Carbonate Sequence Stratigraphy: Recent Developments and Applications vol. 57. American Association of Petroleum Geologists Memoir, pp. 107–131.
Haq, B.U., Hardenbol, J., Vail, P.R., 1987. Chronology of fluctuating sea levels since the Triassic (250 million years ago to present). Science 235, 1156–1167.
Hearon, T.E., Rowan, M.G., Lawton, T.F., Hannah, P.T., Giles, K.A., 2014a. Geology and tectonics of Neoproterozoic salt diapirs and salt sheets in the eastern Willouran Ranges, South Australia. Basin Research 27, 183–207.
Hearon, T.E., Rowan, M.G., Giles, K.A., Hart, W.H., 2014b. Halokinetic deformation adjacent to the deepwater auger diapir, Garden Banks 470, northern Gulf of Mexico: testing the applicability of an outcrop-based model using subsurface data. Interpretation 2, 57–76.
Hearon, T.E., Rowan, M.G., Giles, K.A., Kernen, R.A., Gannaway, C.E., Lawton, T.F., Fiduk, J.C., 2015. Allochthonous salt initiation and advance in the northern Flinders and eastern Willouran ranges, South Australia: using outcrops to test subsurface-based models from the northern Gulf of Mexico. American Association of Petroleum Geologists Bulletin 99, 293–331.
Hernaiz-Huerta, P.P., Solé Pont, J., 2000. Las estructuras del diapiro de Salinas de Rosío y del Alto de San Pedro-Iglesias y sus implicaciones en la evolución tectónica de la transversal Burgalesa de la Cordillera Vascocantábrica-Cuenca del Duero. Revista de la Sociedad Geológica de España 13, 3–4.
Hüneke, H., Krienke, K., 2004. Toe-of-slope deposits of a Givetian reef-rimmed platform: provenance of calcareous density-flow deposits (Rabat-Tiflet-zone, Morocco). Facies 50, 327–346.
Jaillard, E., Dumont, T., Ouali, J., Bouillin, J.-P., Chihaoui, A., Latil, J.-L., Arnaud, H., Arnaud-Vanneau, A., Zghal, I., 2013. The Albian tectonic "crisis" in Central Tunisia: nature and chronology of the deformations. Journal of African Earth Sciences 85, 75–86.
Janson, X., Kerans, C., Bellian, J.A., Fitchen, W., 2007. Three-dimensional geological and synthetic seismic model of Early Permian redeposited basinal carbonate deposits, Victorio Canyon, west Texas. American Association of Petroleum Geologists Bulletin 91, 1405–1436.
Janson, X., Kerans, C., Loucks, R., Marhx, M.A., Reyes, C., Murguia, F., 2011. Seismic architecture of a lower cretaceous platform-to-slope system, Santa Agueda and Poza Rica fields, Mexico. American Association of Petroleum Geologists Bulletin 95, 105–146.
Jo, A., Eberli, G.P., Grasmueck, M., 2015. Margin collapse and slope failure along southwestern Great Bahama Bank. Sedimentary Geology 317, 43–52.
Keim, L., Schlager, W., 2001. Quantitative compositional analysis of a Triassic carbonate platform (Southern Alps, Italy). Sedimentary Geology 139, 261–283.
Kendall, C.G., Schlager, W., 1981. Carbonates and relative changes in sea level. Marine Geology 44, 181–212.
Kenter, J.A.M., 1990. Carbonate platform flanks: slope angle and sediment fabric. Sedimentology 37, 777–794.
Kernen, R.A., Giles, K.A., Rowan, M.G., Lawton, T.F., Hearon, T.E., 2012. Depositional and Halokinetic-Sequence Stratigraphy of the Neoproterozoic Wonoka Formation Adjacent to Patawarta Allochthonous Salt Sheet, Central Flinders Ranges, South Australia. In: Archer, S.G., Alsop, G.I., Hartley, A.J., Grant, N.T., Hodgkinson, R. (Eds.), Salt Tectonics, Sediments and Prospectivity vol. 363. Geological Society of London, Special Publications, pp. 81–105.
López-Horgue, M., Owen, H., Aranburu, A., Fernández-Mendiola, P., García-Mondéjar, J., 2009. Early late Albian (Cretaceous) of the central region of the Basque-Cantabrian Basin, northern Spain: biostratigraphy based on ammonites and orbitolinids. Cretaceous Research 30, 385–400.
López-Horgue, M., Iriarte, E., Schröder, S., Fernández-Mendiola, P., Caline, B., Corneyllie, H., Frémont, J., Sudrie, M., Zerti, S., 2010. Structurally controlled hydrothermal dolomites in Albian carbonates of the Asón valley, Basque Cantabrian Basin, Northern Spain. Marine and Petroleum Geology 27, 1069–1092.
Loucks, R.G., Kerans, C., Janson, X., Rojano, M.M., 2011. Lithofacies analysis and stratigraphic architecture of a deep-water carbonate debris apron: Lower Cretaceous

(latest Aptian to latest Albian) Tamabra Formation, Poza Rica field area, Mexico. In: Shipp, R.C., Weimer, P., Posamentier, H.W. (Eds.), Mass-transport deposits in deep-water settings vol. 96. Special Publications, Society for Sedimentary Geology (SEPM), pp. 367–389.
Mathey, B., 1987. Les Flyschs Crétacé supérieur des Pyrénées Basques: âge, anatomie, origine du matériel, milieu de dépôt et la relation avec l'ouverture du Golfe de Gascogne. Thèse de Doctorat d'Etat. Université de Bourgogne, Dijon, p. 403.
Martín-Chivelet, J., Berástegui, X., Rosales, I., Vilas, L., Vera, J., Caus, E., Gräfe, K., Mas, R., Puig, C., Segura, M., Robles, S., Floquet, M., Quesada, S., Ruiz-Ortiz, P., Fregenal-Martínez, M., Salas, R., Arias, C., García, A., Martín-Algarra, A., Meléndez, M., Chacón, B., Molina, J., Sanz, J., Castro, J., García-Hernández, M., Carenas, B., García-Hidalgo, J., Gil, J., Ortega, F., 2002. Cretaceous. In: Gibbons, W., Moreno, T. (Eds.), The Geology of Spain. Geological Society of London, London, pp. 255–292.
Moore, C.H., 1989. Carbonate Diagenesis and Porosity. Elsevier, Amsterdam.
Mulder, T., Ducassou, E., Eberli, G., Hanquiez, V., Gonthier, E., Kindler, P., Principaud, M., Fournier, F., Léonide, P., Billeaud, I., Marsset, B., Reijmer, J., Bondu, C., Joussiaume, R., Pakiades, M., 2012a. New insights into the morphology and sedimentary processes along the western slope of Great Bahama Bank. Geology 40, 603–606.
Mulder, T., Ducassou, E., Gillet, H., Hanquiez, V., Tournadour, E., Combes, J., Eberli, G., Kindler, P., Gonthier, E., Conesa, G., Robin, C., Sianipar, R., Reijmer, J., François, A., 2012b. Canyon morphology on a modern carbonate slope of the Bahamas: evidence of regional tectonic tilting. Geology 40, 771–774.
Mullins, H.T., Cook, H.E., 1986. Carbonate apron models: alternatives to the submarine fan model for paleoenvironmental analysis and hydrocarbon exploration. Sedimentary Geology 48, 37–79.
Mullins, H.T., Neuman, A.C., 1979. Deep carbonate bank margin structure and sedimentation in the Northern Bahamas vol. 27. Special Publication, Society for Sedimentary Geology (SEPM), pp. 465–492.
Mullins, H.T., Heath, K.C., Van Buren, H.M., Newton, C.R., 1984. Anatomy of a modern open-ocean carbonate slope: northern little Bahama Bank. Sedimentology 31, 141–168.
Orszag-Sperber, F., Harwood, G., Kendall, A., Purser, B., 1998. A review of the evaporites of the Red Sea-Gulf of Suez rift. In: Purser, B.H., Bosence, D. (Eds.), Sedimentation and Tectonics in Rift Basins Red Sea:-Gulf of Aden. Springer, Netherlands, pp. 409–426.
Payros, A., Pujalte, V., 2008. Calciclastic submarine fans: An integrated overview. Earth-Science Reviews 86, 203–246.
Pirazzoli, P., Reyss, J.-L., Fontugne, M., Haghipour, A., Hilgers, A., Kasper, H., Nazari, H., Preusser, F., Radtke, U., 2004. Quaternary coral-reef terraces from Kish and Qeshm Islands, Persian Gulf: new radiometric ages and tectonic implications. Quaternary International 120, 15–27.
Playton, T., 2008. Characterization, variations, and controls of reef-rimmed carbonate foreslopes Ph.D. thesis University of Texas, Austin, USA.
Playton, T.E., Kerans, C., 2002. Slope and toe-of-slope deposits shed from a late Wolfcampian tectonically active carbonate ramp margin. Transactions. Gulf Coast Association of Geological Societies 52, 811–820.
Playton, T.E., Kerans, C., 2015. Late Devonian carbonate margins and foreslopes of the Lennard Shelf, Canning Basin, Western Australia, part A: development during backstepping and the aggradation-To-progradation transition. Journal of Sedimentary Research 85 (11), 1334–1361.
Playton, T.E., Janson, X., Kerans, C., 2010. Carbonate slopes. In: James, N.P., Dalrymple, D.W. (Eds.), Facies Models 4. Geological Association of Canada, St. Johns, Newfoundland, pp. 449–476.
Pomar, L., 2001. Types of carbonate platforms: a genetic approach. Basin Research 13, 313–334.
Pomar, L., Hallock, P., 2008. Carbonate factories: A conundrum in sedimentary geology. Earth-Science Reviews 87, 134–169.
Poprawski, Y., Basile, C., Agirrezabala, L.M., Jaillard, E., Gaudin, M., Jacquin, T., 2014. Sedimentary and structural record of the Albian growth of the Bakio salt diapir (the Basque Country, Northern Spain). Basin Research 26, 746–766.
Principaud, M., Mulder, T., Gillet, H., Borgomano, J., 2015. Large-scale carbonate submarine mass-wasting along the northwestern slope of the Great Bahama Bank (Bahamas): morphology, architecture, and mechanisms. Sedimentary Geology 317, 27–42.
Pujalte, V., Robles, S., Garcia-Mondéjar, J., 1986. Caracteristicas sedimentológicas y paleogeográficas del fan-delta albiense de la Formación Monte Grande y sus relaciones con el Flysh Negro (Arminza-Górliz, Vizcaya). Acta Geologica Hispánica 21, 141–150.
Quintà, A., Tavani, S., Roca, E., 2012. Fracture Pattern Analysis as a Tool for Constraining the Interaction between Regional and Diapir-Related Stress Fields: Poza de La Sal Diapir (Basque Pyrenees, Spain). In: Archer, S.G., Alsop, G.I., Hartley, A.J., Grant, N.T., Hodgkinson, R. (Eds.), Salt Tectonics, Sediments and Prospectivity vol. 363. Geological Society of London, Special Publications, pp. 521–532.
Rat, P., 1988. The Basque-Cantabrian basin between the Iberian and European plates: some facts but still many problems. Revista de la Sociedad Geológica de España 1, 327–348.
Ribes, C., Kergaravat, C., Bonnel, C., Crumeyrolle, P., Callot, J.P., Poisson, A., Temiz, H., Ringenbach, J.-C., 2015. Fluvial sedimentation in a salt-controlled mini-basin: stratal patterns and facies assemblages, Sivas Basin, Turkey. Sedimentology 62, 1513–1545.
Robador, A., Garcia-Mondéjar, J., 1987. Caracteres sedimentológicos generales del "Flysch-Negro" entre Baquio y Guernica (Albiense superior-Cenomaniense Inferior, provincia de Vizcaya). Acta Geologica Hispánica 21, 275–282.
Robles, S., Pujalte, V., Garcia-Mondéjar, J., 1988. Evolución de los sistemas sedimentarios del margen continental Cantábrico durante el Albiense y Cenomaniense, en la transversal del litoral vizcaino. Revista de la Sociedad Geológica de España 1, 3–4.
Robles, S., Garrote, A., García-Mondéjar, J., 1989. XII Congreso Español de Sedimentología: Simposios y conferencias. Universidad del País Vasco, Departamento de Estratigrafía, Geodinámica y Paleontología, Bilbao.
Roca, E., Muñoz, J.A., Ferrer, O., Ellouz, N., 2011. The role of the Bay of Biscay Mesozoic extensional structure in the configuration of the Pyrenean orogen: constraints from the MARCONI deep seismic reflection survey. Tectonics 30, TC2001.
Rosales, I., 1999. Controls on carbonate-platform evolution on active fault blocks: the Lower Cretaceous Castro Urdiales platform (Aptian-Albian, Northern Spain). Journal of Sedimentary Research 69, 447–465.
Rowan, M.G., Lawton, T.F., Giles, K.A., Ratliff, R.A., 2003. Near-salt deformation in La Popa basin, Mexico, and the Northern Gulf of Mexico: A general model for passive diapirism. American Association of Petroleum Geologists Bulletin 87, 733–756.
Rowan, M.G., Lawton, T.F., Giles, K.A., 2012a. Anatomy of an Exposed Vertical Salt Weld and Flanking Strata, La Popa Basin, Mexico. In: Archer, S.G., Alsop, G.I., Hartley, A.J., Grant, N.T., Hodgkinson, R. (Eds.), Salt Tectonics, Sediments and Prospectivity vol. 363. Geological Society of London, Special Publications, pp. 33–57.
Rowan, M.G., Giles, K.A., Roca, E., Arbues, P., Ferrer, O., 2012b. Analysis of Growth Strata Adjacent to an Exposed Deepwater Salt Diapir, northern Spain. American Association of Petroleum Geologists Annual Convention, Long Beach, USA.
Saller, A.H., 1996. Differential compaction and basinward tilting of the prograding capitan reef complex, Permian, west Texas and southeast New Mexico, USA. Sedimentary Geology 101, 21–30.
Saura, E., Vergés, J., Martín-Martín, J.D., Messager, G., Moragas, M., Razin, P., Grélaud, C., Joussiaume, R., Malaval, M., Homke, S., Hunt, D.W., 2014. Syn- to post-rift diapirism and minibasins of the Central High Atlas (Morocco): the changing face of a mountain belt. Journal of the Geological Society 171, 97–105.
Savary, B., Ferry, S., 2004. Geometry and petrophysical parameters of a calcarenitic turbidite lobe (Barremian-Aptian, Pas-de-la-Cluse, France). Sedimentary Geology 168, 281–304.
Schultz-Ela, D.D., 2003. Origin of drag folds bordering salt diapirs. American Association of Petroleum Geologists Bulletin 87, 757–780.
Serrano, A., Martínez del Olmo, W., 1989. Diapirismo del Trías Salino en el Dominio Cántabro–Navarro. Libro homenaje a Rafael Soler, pp. 115–121.
Skelton, P.W., Gili, E., 2012. Rudists and carbonate platforms in the Aptian: a case study on biotic interactions with ocean chemistry and climate. Sedimentology 59, 81–117.
Spence, G.H., Tucker, M.E., 1997. Genesis of limestone megabreccias and their significance in carbonate sequence stratigraphic models: a review. Sedimentary Geology 112, 163–193.
Talling, P.J., Masson, D.G., Sumner, E.J., Malgesini, G., 2012. Subaqueous sediment density flows. Sedimentology 59, 1937–2003.
Tournadour, E., Mulder, T., Borgomano, J., Hanquiez, V., Ducassou, E., Gillet, H., 2015. Origin and architecture of a mass transport complex on the northwest slope of Little Bahama Bank (Bahamas): relations between off-bank transport, bottom current sedimentation and submarine landslides. Sedimentary Geology 317, 9–26.
Tucker, M.E., Wright, V.P., 2009. Carbonate Sedimentology. John Wiley and Sons.
Vail, P.R., Mitchum Jr., R.M., Todd, R.G., Widmier, J.M., Thompson III, S., Sangree, J.B., Bubb, J.N., Hatlelid, W.G., 1977. Seismic Stratigraphy and Global Changes of Sea-Level. In: Payton, C.E. (Ed.)Seismic Stratigraphy-Applications to Hydrocarbon Exploration vol. 26. American Association of Petroleum Geologists Memoir, pp. 49–212.
Vergés, J., Saura, E., Messager, G., Martín-Martín, J.D., Moragas, M., Razin, P., Grelaud, C., Joussiaume, R., Malaval, M., Hunt, D., 2013. The Central High Atlas in Morocco: A Snapshot of a Jurassic Diapiric Rifted Basin. American Association of Petroleum Geologists Annual Convention and Exhibition, Denver, USA.
Verwer, K., Merino-Tomé, O., Kenter, J.A., Della Porta, G., 2009. Evolution of a high-relief carbonate platform slope using 3D digital outcrop models: Lower Jurassic Djebel Bou Dahar, High Atlas, Morocco. Journal of Sedimentary Research 79, 416–439.
Vicente-Bravo, J., Robles, S., 1991a. Geometría y modelo deposicional de la secuencia Sollube del Flysch Negro (Albiense medio, norte de Bizkaia). Geogaceta 10, 69–72.
Vicente-Bravo, J., Robles, S., 1991b. Caracterización de las facies de la transición canal-lóbulo en la secuencia Jata del Flysch Negro (Albiense Superior norte de Vizcaya). Geogaceta 10, 72–75.
Voort, H., 1964. Zum flyschproblem in den Westpyrenäen. Geologische Rundschau 53, 220–233.
Wiedmann, J., Boess, J., 1984. Ammoniten funde aus der Biskaya-synkline (nordspanien)-kreidegliederung und alter des kreide-vulkanismus. Eclogae Geologicae Helvetiae 77, 483–510.